2013

External Control Interface, Dynamic Modeling and Parameter Estimation of a Research Treadmill

Omer Sirin
Cleveland State University

EXTERNAL CONTROL INTERFACE, DYNAMIC MODELING AND PARAMETER ESTIMATION OF A RESEARCH TREADMILL

Omer Sirin

Bachelor of Science in Mechatronics Engineering

Bahcesehir University

Istanbul, Turkey July, 2012

submitted in partial fulfillment of requirements for the degree

MASTERS OF SCIENCE IN BIOMEDICAL ENGINEERING

at the

CLEVELAND STATE UNIVERSITY

August, 2013

This thesis has been approved
for the department of CHEMICAL AND BIOMEDICAL
ENGINEERING
and the College of Graduate Studies by:

Thesis Chairperson, Hanz Richter, Ph.D.

Department & Date

Sridhar Ungarala, Ph.D.

Department & Date

Daniel Simon, Ph.D.

Department & Date

ACKNOWLEDGMENTS

I would like to express my gratitude to my advisor Dr. Hanz Richter, who provided guidance and essential support. His useful comments, remarks and engagement through the learning process of this master thesis,improved my research skills and preparad me for future challenges.I would also like to thank Dr. Sridhar Ungarala and Dr. Daniel Simon for being in my thesis committee. Furthermore, I would like to thank Hadis Mohammadi, Oguz Ciftci, Maulik Kalolia for their assistance to this project. Thanks to all my friends and my family who have encouraged, supported and helped me endure all stress of last two years.

EXTERNAL CONTROL INTERFACE, DYNAMIC MODELING AND PARAMETER ESTIMATION OF A RESEARCH TREADMILL

Omer Sirin

ABSTRACT

Treadmills providing linear continuous movement are used for robotic testing of prostheses in order to study their operating characteristics. However, traditional exercise treadmills are not able to simulate various conditions such as avoiding an obstacle, climbing, descending, reversing direction, or stopping instantly. The focus of this thesis is to examine control algorithms (position, speed and force) for the drive mechanism of a research treadmill to fulfill the gap in the situations described above. The system consists of a power supply, a computer with Matlab, and the treadmill that includes a DC motor, a pulley and belt. Also, an external encoder is installed on the motor to measure the position of the belt. The bond graph method is used to model the system to find the symbolic transfer function. Simultaneously, system identification techniques are used to estimate a numeric transfer function. Some parameters of the model are experimentally measured, and the rest are extracted by matching two transfer functions. Control algorithms such as proportional-integral-derivative and sliding mode are implemented in the system for simulation and real-time operation. The results demonstrate that this system is suitable for producing motion paths that traditional treadmills cannot, and it can handle difficult-to-model situations such as the synchronized movement of the treadmill with a prosthesis-testing robot.

TABLE OF CONTENTS

LIST OF FIGURES

LIST OF TABLES

CHAPTER I

INTRODUCTION

This chapter provides information about the motivation for this thesis and a review of the literature. It also discusses current research treadmill technologies and their limitations. The aim of this project is discussed in the objective section. Likewise, the thesis structure is provided.

1.1 Motivation and Literature Review

When it comes to walking, running or other continuous motions performed by humans, the routine locomotion of daily ambulation is a continuous acceleration and deceleration with movement along curvilinear paths. Even when making an attempt to move at a nearly constant speed and on a linear walkway in situations of a prolonged gait, humans tend to display an unsteady progression in speed and direction. If this anomaly is to be studied in a viable fashion to understand mechanical, metabolic, neuromuscular and psychological determinants of such random fluctuations in speed and other factors, test treadmills must not be restricted to move at a constant speed [12]. Traditional exercise treadmills are not capable of simulating other than a constant speed. This was the motivation to implement a controller for the treadmill used for robotic testing of prostheses.

Human body-effort limit tests for mobility rehabilitation, and regenerative medicine have been successful in tandem with treadmills that were usually intended for use in sports and recreational aims, but studied further for the aforementioned medical uses in a study done by Stavar *et al.* [18]. These tests illustrate that a person who has locomotion dysfunction can benefit from a treadmill that can adapt gradually to assist in the needs of the subjects rehabilitation. When the motion velocity and system accelerations are monitored and parameters are controlled precisely, the system can respond to the users' locomotion and assist them in a free, unrestricted manner [18]. This was a motivation to implement PID controller and a robust control called sliding mode control in order to get an opportunity to provide different motion pathways such as acceleration.

Another consideration to this widely expanding experimental field can be observed in the aspects of robotics as evidenced by a study done by Von Zitzewitz *et al.* [20]. This study suggests that robot-aided treadmills can be a useful treatment method for patients with locomotive dysfunctions. Currently, treadmills for rehabilitation purpose perform constant speeds or speeds adjusted manually by therapists. They provide a controller that allow patient cooperation and also it can be extended to simulate different walking conditions, such as inclined or declined directional ambulation [20]. As a motivation, a controller can be introduced to overcome the limitation of commercial treadmills. This controller can provide an option to adjust their own gait speed by the user.

The control of treadmill can be a valuable tool for variety of research studies. It can be used in a research for avoiding inertial force due to the acceleration [4]. In research about gait rehabilitation robots, a constant speed treadmill was a limitation [7] and a controlled treadmill would provide other pathways to the research. A controlled treadmill can be used in research for training to reduce falls in Parkinson's disease [13]. A controlled treadmill can provide forward, backward drive and instant

stop to disturb the subject's standing balance. A treadmill speed can be synchronized with virtual environments for gait training of poststroke [9]. The treadmill can be also controlled to provide smooth and gradual changes in velocity and acceleration [16]. Electromyography activity of a leg can be examined while a treadmill moves sinusoidal fashion backward and forward, with a subject standing on it. Different frequencies between 0.5 Hz and 0.3 Hz can be applied [5]. Treadmill can be controlled to use in virtual environments [10]. In our project, these research topics were the motivation, because of the fact that many motion profiles can be simulated with a treadmill.

Robotic testing of prosthesis is an important tool in extracting dynamic characteristics of prosthetic body implants such as knees. It can protect human subjects from hazardous conditions and provide useful data gathering due to ease of repeatability [15]. In order to examine the characteristics, different walking speeds, accelerations, decelerations and pathways are required. For example, the robotic leg and treadmill are fixed to the ground and if it is desired to examine backwards walking, the treadmill belt needs to be driven backwards.

Some literature and technology reviews were collected for this thesis research. Different approaches have been provided by researchers in order to bring a solution for simulating alternative gait pathways that traditional treadmills cannot.

In the experiment conducted by Minetti *et al.*, the acceleration or deceleration of the subject are captured by a sensor and collected data is processed to drive treadmill in real time. Self-selected speeds of walking or running are estimated by the system. Test errors caused by bias are minimized by feedback system. In this research, one of the conclusions was that the treadmill with control system triggers the subjects to use slightly higher speeds than in a experiment on a walkway [12]. In our system, the improved control will contribute to smoother walking experiences that will minimize tracking errors. In addition, obstacle avoidance conditions can be included to the

research and the response of the subjects can be examined by controlling the belt position.

Stavar *et al.* introduced an aproach to reconfigure a classic treadmill to simulate different conditions such as backward and forward with alternative speeds, accelerations, and inertial moments. In this research, the initial control system is overridden and an adaptive control system was implemented to estimate direction and speed. Also a tracking system is integrated into the control system. The treadmill motor was controlled using a PID controller which was tuned by empirical methods. Finally, in their experiment, they tested their controller without load [18]. Compared to their work, a finer speed control can be accomplished in this thesis due to the fact that an optical encoder is used measure the speed. In contrast, this thesis uses model-based approach where the model is obtained from a combination of bond graph and system identification techniques. Also, the tests were conducted with a subject in our system. Finally, the overall intention was to research and develop a complete virtual locomotion system with application in actual and future of interest as our goal.

Zitzewitz *et al.* used a treadmill that included a hardware-implemented PID speed controller. In that research, system identification was performed to determine the dynamics of the PID-controlled treadmill. The transfer function of the PID-controlled treadmill was found to be approximately [20]:

$G(s) = \frac{v_(actual(s))}{v_(desired(s))} = e^{-0.08}\frac{1}{0.1s+1}$

In our project system identification toolbox of Matlab is used in order to find transfer function from data that was obtained by applying a swept sinewave (chirp) signal to the system. As a result, a good approximation of transfer function for the system is obtained by choosing two poles and three zeros. Our system is more specific in terms of finding transfer function, so we might have better results. In addition, in our system, sliding mode controller is applied that provided better results than the PID controller.

1.2 Objective and Methods

The main objective of this thesis is to utilize engineering principles in order to provide the simulation of different motion paths that include various conditions such as: avoiding an obstacle, acceleration, deceleration, reversing direction, or stopping instantly. Feasibility tests can be examined by human subjects and robot operated prostheses.

Symbolic transfer functions of the drive mechanism are obtained with bond graphs with the aid of the 20-Sim program [1]. Bond graphs are domain-independent graphical descriptions of the dynamic behavior of physical systems. The systems from different domains (electrical, mechanical, hydraulic, acoustic, thermodynamic, material) are described in the same way. The basis is that bond graphs are based on energy and energy exchange. In addition, system identification toolbox of Matlab is used to supplement direct parameter measurements. A chirp signal was applied to the current servo amplifiers and the resulting velocity recorded. The Matlab System Identification Toolbox is used to subsequently determine a transfer function between control input and belt speed.

Another aspect of this thesis is the estimation of parameters. Some parameters are measured directly. Since the numerical transfer function is available from system identification, parameter matching can be used to find parameters that were not measured directly. A Simulink program is built to implement the PID and sliding mode control.

As a conclusion, the tests are examined and the results are compared.

1.3 Composition of Thesis

This thesis is organized as follows. The experimental setup and block diagram are presented in Chapter 2. The system identification and parameter estimation explained

in Chapter 3. Controller design including simulation of PID and sliding mode control are provided in Chapter 4. Real time experiments are shown in Chapter 5. Finally, conclusion and recommendations are presented in Chapter 6.

CHAPTER II

EXPERIMENTAL SETUP

This chapter gives an overview of the elements involved in the experimental setup and relationship with each other. The function of each element is explained and a block diagram of the system is provided.

2.1 Block Diagram of the System

Figure 2.1 shows the connection between each element in the system. The rotational speed of the cylinder in the motor is read by the encoder attached to the motor. The signal is transmitted from the encoder to computer throughout data acquisition board and the belt speed is calculated. The speed data is processed in a Simulink real-time interface and the control signal is sent to the power amplifier, which drives the DC motor.

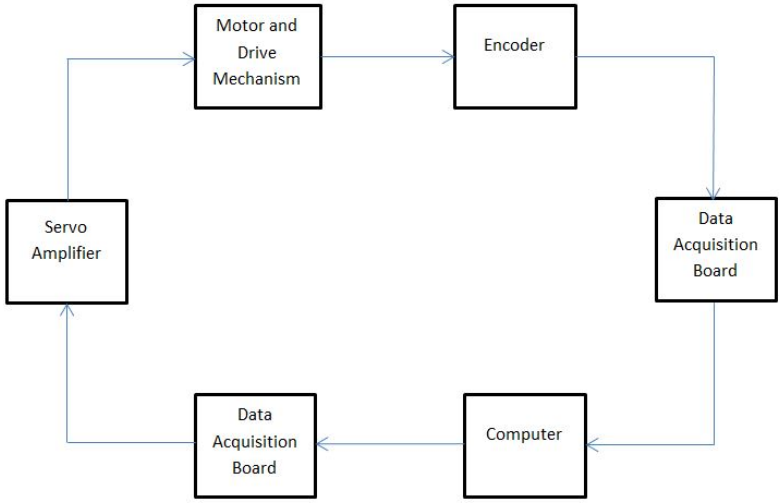

Figure 2.1: Block diagram of the system

2.2 Elements of the System

Figure 2.2 shows the complete system. The system basically consist of a power amplifier, a computer with Matlab, data acquisition board and the treadmill that includes a DC motor, a pulley and belt. Also an external encoder is installed on the motor to measure the position of the belt. Each element in the system will be discussed in following sections individualy in detail.

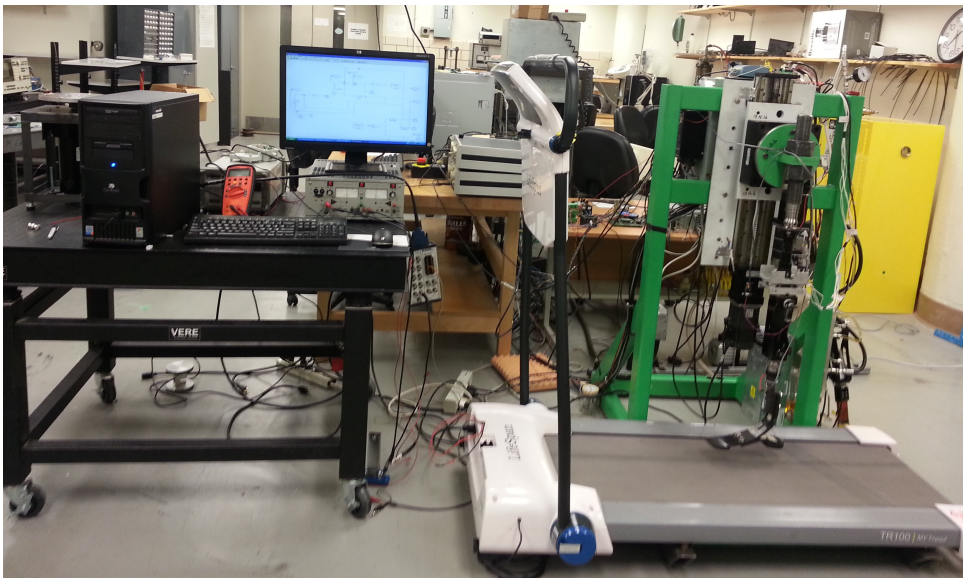

Figure 2.2: Picture of the complete system

2.2.1 Power Amplifier

Figure 2.3 shows the amplifier used in the system to drive motor. Kepco bipolar operational power supply/amplifier is a high-speed power operational amplifier that can be used to provide control voltages for tests and final operation. It is capable of supplying +/- 40 volts at +/- 6 amps.

Figure 2.3: Kepco bipolar operational power supply/amplifier.

2.2.2 Data Acquisition Board and the Connector

Figure 2.4 shows the data acquisition board used in the system. The National Instruments PCI-6259 is a high-speed multifunction M Series data acquisition (DAQ) board optimized for superior accuracy at fast sampling rates. It provides 32 analog inputs at 16 bits, 1MS/s(Mega Samples per second)(Multichannel),1.25 MS/s(1-channel); 4 anolog output at 16 bits, 2.8 MS/s; 48 digital I/O;and 32-bit counters. It has also NI-MCal calibration technology for increased measurement accuracy. Connection for DAQ board is provided by the BNC-2110 connector provides connection of analog signals, some digital signals, and two user-defined connections. It is shown in Figure 2.5.

Figure 2.4: Data acquisition board: The National Instruments PCI-6259

Figure 2.5: The BNC-2110 connector

2.2.3 Treadmill Drive System

Figure 2.6 shows treadmill drive mechanism inludes a motor, two pulleys and a belt. Tewei Engines C8APB1 is the DC motor used in the treadmill. It is rated at 90 volts, 8 amps, 4200 rpm, and 1.5 H.P. A pulley with 1 inch diameter is attached to the motor shaft and it is connected to the pulley whose diameter is 4 inches. The treadmill belt is driven by the bigger pulley with help of a roller mounted in the center of the pulley.

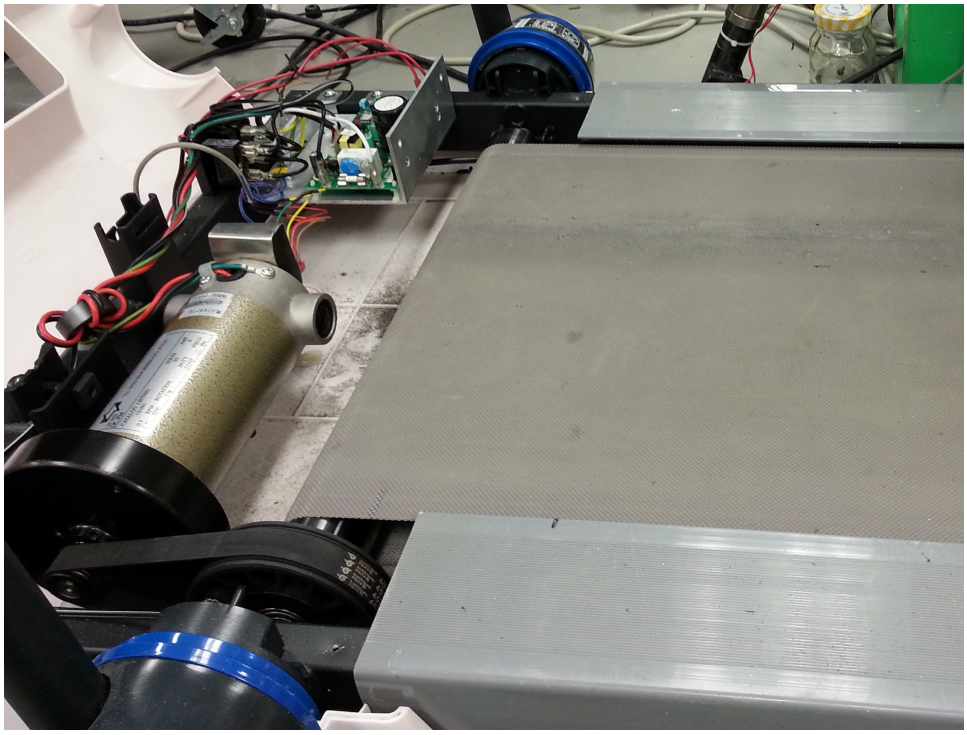

Figure 2.6: Treadmill drive system

2.2.4 Encoder

Figure 2.7 shows the encoder used in the system to measure rotational speed of the cylinder in the motor. Enc1j d28 L00128L is an rotary optical encoder whose resolution is 128 cycles per revolution.

Figure 2.7: Rotary optical encoder: Enc1j d28 L00128L

An aluminum block is bent into its proper shape. The two sides of the block are cut off same wide with diameter of the screws on the motor. The encoder is attached to the aluminum, and then it is fastened to the motor shaft. After encoder mounting, the input of the encoder needs to be introduced to the computer by converting counts to meters to find displacement. A 38 inch length field on the belt is marked, the belt was driven manually and the counts were recorded. The gain that converts counts to meter is found as $3.1055 \times 10^{-4} m/count$. The calibration equation is shown below.

$$Displacement = \frac{counts \times \ 38 \ inch \times 0.0254 \ m/inch}{3108 \ counts} = 3.1055 \times 10^{-4} \ m/count \tag{2.1}$$

2.2.5 Computer and Matlab

Computer with Pentium 4, CPU at 3 GHz, 1 Gb of ram is used for Matlab and Simulink program version 2006b. For real-time experiments a software application called WinCon is used. It was developed by Quanser Consulting Inc. It provides ease and efficient way to run Simulink models in real-time. It is used to read encoder and to run controller model in our project. It allows user to plot real-time data and save it into Matlab.

2.2.6 Leg Prosthesis Test Robot

Prosthetic leg with robotic hip simulator is a device designed for simulating swing and stance trajectories of human gait. It also provides researchers with an opportunity to examine operating characteristics. It is restricted to two degrees of freedom, which are hip vertical displacement and hip swing, in order to repeat two-dimensional gait patterns. It provides a hip displacement amplitudes of up to 50 mm, with a maximum velocity of 1 m/s. Overall machine dimensions are $48'' \times 61'' \times 26''$. The device is shown in Figure 2.8.

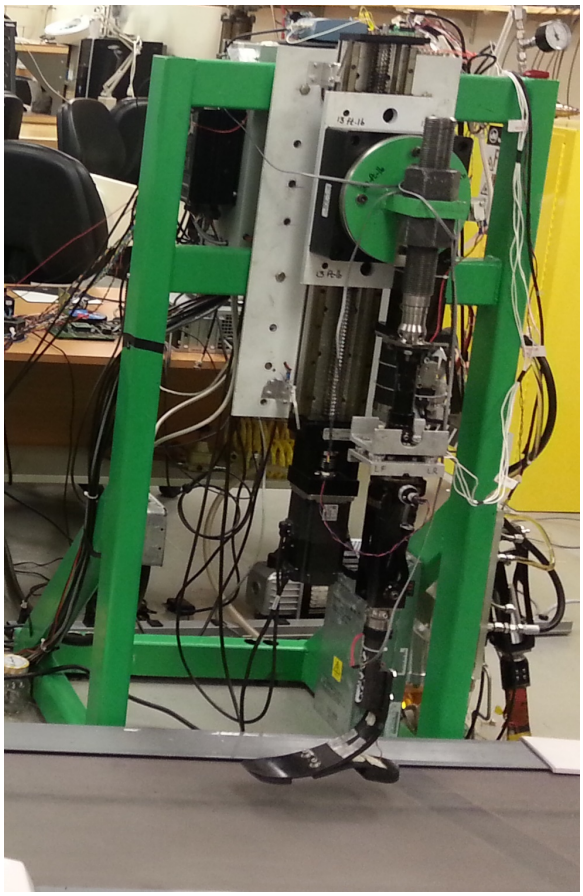

Figure 2.8: Prosthetic leg with robotic hip simulator

CHAPTER III

SYSTEM MODELING AND PARAMETER ESTIMATION

This chapter describes the system modeling process in detail. It explains how system parameters are found. The bond graph method is introduced and it is used in order to find symbolic transfer functions. Simultaneously, Matlab's system identification toolbox is used to find a numeric transfer function of the system. Some of the parameters of the symbolic TF are measured and the rest are found by equalizing two transfer functions. Finally, a step response of the system is genereated to adjust some model gains. The system schematic is shown in figure 3.1.

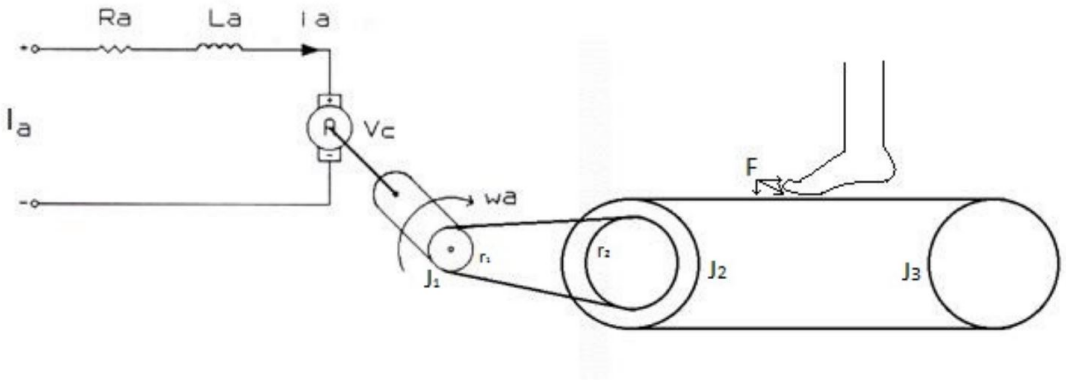

Figure 3.1: System schematic

3.1 System Identification

System identification is a process that uses methods to generate mathematical models of dynamic systems from measured data. The behavior of a real-time systems can be predicted by relating input and output data. It can be useful for estimating unknown parameters of the system.

System identification toolbox of Matlab program provides the user with an opportunity to build mathematical models of a dynamic system from measured input-output data. The toolbox allows the user to adjust parameters such as number of poles and zeros, in order to find maximum likelihood model of the system. There are several basic steps to estimate the model [11].

1. An experiment is conducted and input-output data is recorded to use it in toolbox.

2. After data is imported into toolbox, desired process such as removing means, filtering noise are applied.

3. The candidate models are found by changing the parameters (number of poles, number of zeros, error term)

4. The best model is chosen from data fit results. [11]

A chirp is a constant-amplitude signal in which the frequency changes with time. It is fed to the system in order to collect system response data for use in system identification. Its basic parameters are set as: initial frequency (0.1 Hz), target time (20), and frequency at target time (10Hz). The input of the system was voltage and the output was velocity of the belt. First of all, the data set is introduced to the toolbox, and then the mean is removed. The resulting data is fed as working data for the next operation. Low-pass filtering is then applied to limit the bandwidth of the estimated model. Figure 3.2 shows the input and output signals and processed

signals. Two alternatives were tried for the system: first order TF and second order TF. For the first order TF, the parameters are set as: number of pole (1), number of zeros (1), error term (0). The resulting estimation gave a 55.9% match. For the second order TF, the orders are set as: number of poles (2), number of zeros (2), error term (0). The resulting estimation gave 85.53% match. It was decided to use second order system due to better prediction. The TF of the system from input voltage to output belt velocity was extracted, and it is shown below.

$$TF = \frac{30.28744}{s^2 + 27.14s + 174.9}\left(\frac{m}{Vs}\right) \tag{3.1}$$

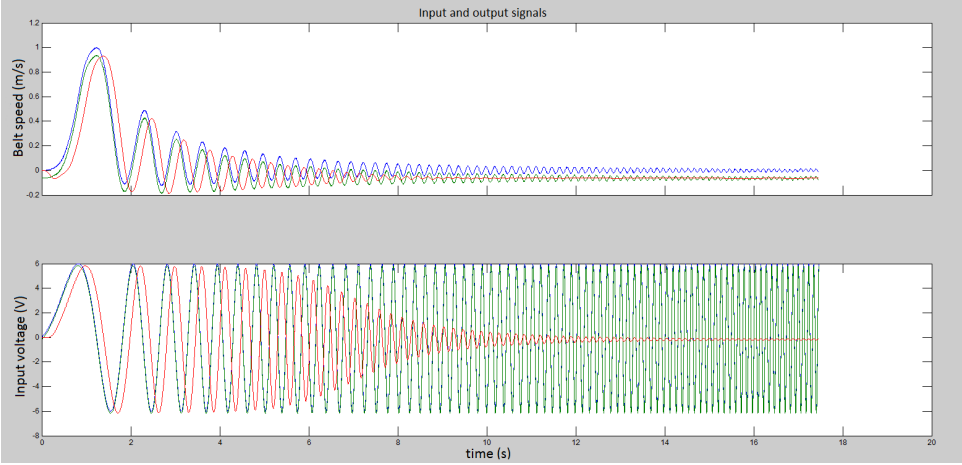

Figure 3.2: The input and the output signals.The blue line represents pure signal, the green line represents the signal after removing mean, and the red line represents the final signal after it was filtered.

3.2 Motor Dynamics

In this section, the dynamics of a DC motor is analyzed in some detail. The DC motor simply consists of a stator and rotor. A current carrying conductor in a magnetic field provides a force $F = i\Phi$, where Φ is the magnetic flux and i is the current in the conductor. When the stator produces a radial magnetic flux and the current in the

armature, then this creates a torque on the rotor causing it to rotate. This results in the equation:

$$\tau_m = \alpha i_a \tag{3.2}$$

where τ_m is the motor torque (N-m), α is the torque constant, and i_a is the armature current (amperes).

When a conductor turns in a magnetic field, a voltage V_b is created, called back emf.

$$V_b = \alpha w_m \tag{3.3}$$

where V_b is the back emf (volts), w_m is the angular velocity of the rotor (rad/sec), and α is the same used in the torque equation.

The parameters that will be useful while creating a bond graph of the system are listed below [17].

- V: armature voltage
- L: armature inductance
- R: armature resistance
- V_b: back-emf
- i_a:armature current
- τ_m:generated torque [17]

3.3 Bond Graph Method

In this section, the bond graph method is briefly described. The implementation of the bond graph in the system is shown.

Bond graphs depict the dynamic behavior of physical systems that have different domains such as electrical, mechanical, hydraulic etc. The bond graph method is

a powerful tool based on energy and energy exchange for modeling an engineering system [3].

3.3.1 Bonds and Ports

Two elements of a system are connected with a single line called bond. This bond shows a power flow which enters on one side and leaves at the other one between the two connected elements. The product of two variables such as voltage and current creates the physical dimension of power. In each physical domain, there is such a combination of variables. For example, in mechanical systems, they are force and velocity for translation, and torque and angular velocity for rotation, and in hydraulics, it is pressure and volume flow, and in thermodynamic systems, they are temperature and rate of change of entropy [3].

3.3.2 Bond Graph Elements

Bond graph elements are symbolized with letter combinations that designate the type of element. The bond graph elements are listed as [3]:

- C is the storage element of q-type variable, for example a capacitor that stores charge, and a spring which stores displacement.
- I is the storage element of a p-type variable, for example an inductor which stores flux linkage,and a mass that stores momentum.
- R indicates a resistor which dissipating free energy, for example an electric resistor, and mechanical friction.
- Se and Sf are sources, for example voltage source in electric system, force source as gravity, and flow source such as pump.
- TF is transformer, e.g. an electric transformer, pulleys.

- GY is gyrator, e.g. electromotor, centrifugal pump.
- 0 and 1 are junctions, for connecting two or more elements.

3.3.3 Bond Graph of the System

The 20-Sim program [1] is used to draw the bond graph shown in Figure 3.3 and obtain relevant transfer functions in symbolic form.

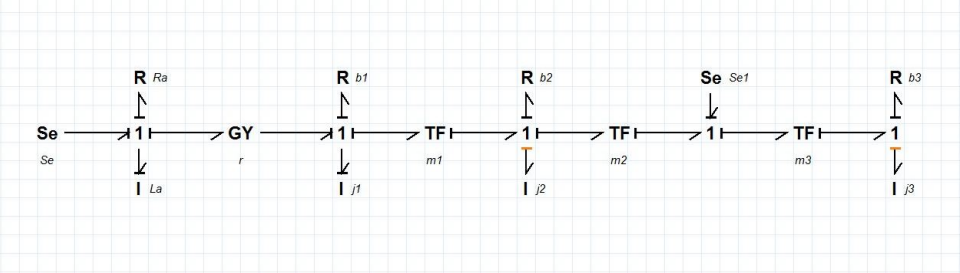

Figure 3.3: Bond graph of the system

- Se_1: Source of effort (Voltage)
- R_a: armature resistance
- L_a: armature inductance
- r: torque constant
- b_1: motor damping
- J_1: moment of inertia of the rotor
- m_1: ratio of two pulleys= r_1/r_2
- b_2: damping of roller connected to the bigger pulley
- J_2: moment of inertia of roller connected to the bigger pulley
- m_2: radius of bigger pulley (transforms rotational to linear)

- Se_1: Source of effort (Force caused by leg)
- m_3: inverse of radius of bigger pulley (transforms linear to rotational)
- b_3: damping of the free turning roller
- J_3: moment of inertia of the free turning roller

A TF for the system is generated by choosing input as Se (volts) and output as flow (belt velocity) at the Se1 junction. The second order TF is found as:

$$TF = \frac{\alpha m_1 m_2}{as^2 + bs + c} \tag{3.4}$$

where

$a = I_a j_1 + I_a j_2 m_1^2 + I_a j_3 m_1^2 + I_a j_3 m_1^2 m_2^2 m_3^2$

$b = I_a b_1 + R_a j_1 + I_a b_2 m_1^2 + R_a {j_2}_{m_1}^2 + I_a b_3 m_1^2 m_2^2 m_3^2 + R_a j_3 m_1^2 m_2^2 m_3^2$

$c = \alpha^2 + R_a b_1 + R_a b_2 m_1^2 + R_a b_3 m_1^2 m_2^2 m_3^2$

3.3.4 Parameter Estimation

The radius of the pulleys are measured directly, so that $m1$ and $m2$ can be calculated. The torque constant (α) was measured by correlating the speed of the belt to the DC machine terminal voltage when operating in generator mode. The armature resistance (Ra) and the armature inductance (La) are measured by multimeter. After finding these individual parameters, the other parameters such as a,b,c are extracted by equalizing the second order transfer function found from system identification toolbox to that obtained from the bond graph method.

- $r_1 = 0.5$ inch (0.0127 m)
- $r_2 = 2$ inches (0.0508 m)
- $m_1 = \frac{1}{4} = 0.25$

- $m_2 = 0.0508$ m
- $r = \alpha = \frac{V}{w} = 0.031\ \frac{Nm}{A}$

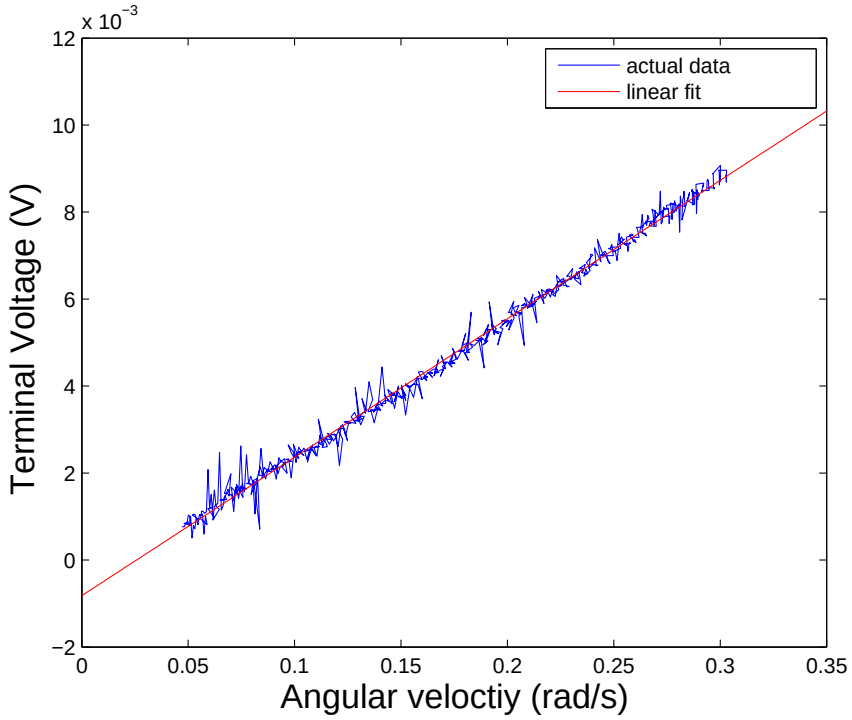

Figure 3.4: Estimation of torque constant

- $Ra = 3.3\ \Omega$
- $La = 3.13$ mH
- $a = 2.846406953 \times 10^{-7}\ \frac{Nms^3}{A}$
- $b = 4.416894495 \times 10^{-6}\ \frac{Nms^2}{A}$
- $c = 1.627448229 \times 10^{-5}\ \frac{Nms}{A}$

3.3.5 TF From Disturbance Force to Belt Velocity

Although system identification alone gives a numeric transfer function that can be used for control design, the effect of load disturbance is given by Eq (3.5). This TF

could not be measured using system identification with the available instrumentation. The bond graph method was used to extract TF from disturbance force caused by the leg to belt velocity. This results in the following TF:

$$TF = \frac{m_1^2 m_2^2 (R_a + I_a s)}{as^2 + bs + c} \tag{3.5}$$

where

$$a = I_a j_1 + I_a j_2 m_1^2 + I_a j_3 m_1^2 + I_a j_3 m_1^2 m_2^2 m_3^2$$

$$b = I_a b_1 + R_a j_1 + I_a b_2 m_1^2 + R_a j_{2m_1}{}^2 + I_a b_3 m_1^2 m_2^2 m_3^2 + R_a j_3 m_1^2 m_2^2 m_3^2$$

$$c = \alpha^2 + R_a b_1 + R_a b_2 m_1^2 + R_a b_3 m_1^2 m_2^2 m_3^2$$

CHAPTER IV

CONTROLLER DESIGN

In this chapter controller design is discussed. Two types of controller are used in this project. First of all, PID controller which is a well known controller is described briefly. The second approach which is a more advanced method called sliding mode controller is outlined and applied to the treadmill system.

4.1 PID Controller

Proportional-integral-derivative (PID) controller is a widely-used tool in industry due to its good performance and simplicity [6]. The tree parameters define control action: the proportional term provides an action according to error magnitude, which means the bigger error, the bigger the correction. The integral term provides correction according to error persistence, which means the longer error continues, the bigger the correction. Finally, the derivative term produces an action according to the change of error with respect to time, which means the faster error is changing, the bigger the correction. P, PI, PD, or PID can be used in a control system as desired [2]. The transfer function of PID controller is as following:

$$G_c(s) = K_p + \frac{K_i}{s} + K_D s \tag{4.1}$$

PID gains may be determined by manual tuning based on observation and experience and by other methods. The Ziegler-Nichols method is a popular way to tune PID gains [14]. For various industrial systems, the effects of the PID gains on system response are summarized in Table 4.1.

PID Gain	Percent Overshoot	Settling Time	Steady-State Error
Increasing K_P	Increases	Minimal effect	Decreases
Increasing K_I	Increases	Increases	Zero steady-state error
Increasing K_D	Decreases	Decreases	No impact

Table 4.1: Effects of the PID Gains on the Step Response

A Simulink model of system for the treadmill with PID controller is shown in Figure 4.1. A step input is fed into the system and the PID gains are tuned manually as: proportional (100), integral (0.18), derivative (0). The step response of system shown in Figure 4.2.

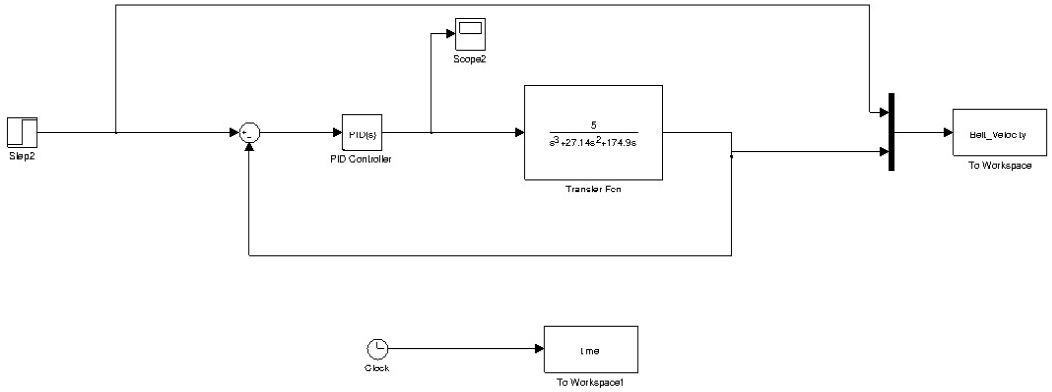

Figure 4.1: Model of the system with PID controller

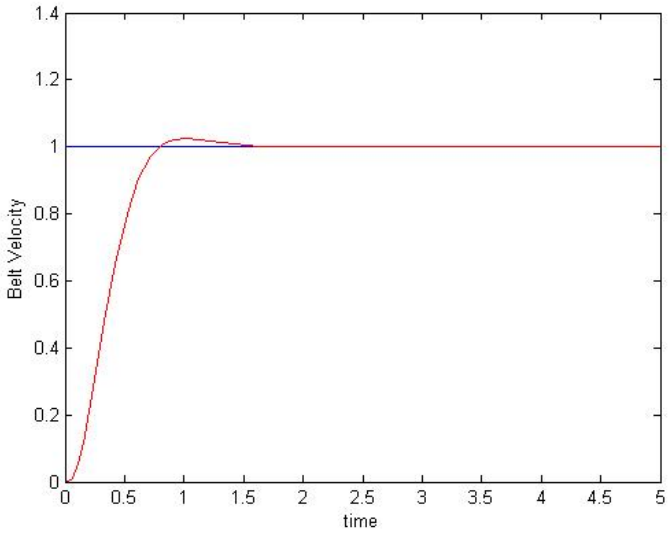

Figure 4.2: Step response of PID simulation

4.2 Sliding Mode Control

Sliding mode control (SMC) is recently one of the most important tools with applications in different areas of control engineering. The most important applications that we can mention for sliding mode control are in power electronics, robotics and motion control. SMC is a control method that changes the dynamics of a system by forcing the system state to "slide" along a surface defined by a function of the state variables. It can switch from one continuous structure to another based on the current position in the state space. Hence, sliding mode control is a variable structure control method [19].

Sometimes the trajectory of the system moves to a region with different control structure so the control law which was working for one region is not working for another. In some applications like the ones that they need a robot operating in interaction with an environment with alternative features, robot needs to follow different trajectories as environment changes, so we need to have different controls on different

trajectories, another word control law is entering different regions of controls. By using sliding mode control, the control will slide along the boundaries of the different regions. The motion of the system as it slides along these boundaries is called a sliding mode and the geometrical locus consisting of the boundaries is called the sliding (hyper) surface. In robot application using sliding mode control, choosing an appropriate sliding surface is important since using an inappropriate sliding surface can lead to chatter, energy loss, plant damage, and excitation of unmodeled dynamics with higher frequencies [8].

The main features of sliding mode control are:

- Reduction in the order of the system while on the sliding mode
- Robustness property against certain disturbances.

The main benefit of SMC is the independence from uncertainties and disturbances while the system is in sliding mode. The state trajectory remains near the sliding surface and even by going from one region of control to another one by switching of the control law, the state trajectory tends toward the sliding surface. While modeling a plant there will always be a difference between the actual model and the mathematical model so by using sliding mode control exploiting its robustness property we can overcome modelling errors [8].

Sliding mode controllers can be used in different applications with different purposes. One of sliding mode controllers application is controlling of electric drives equipped with switching power converters. Since there is the discontinuous operation mode for power converters need to defining a discontinuous sliding mode controller is vital for the system. Sliding mode control also can be used in designing of state observers. By using sliding mode control in designing sliding mode observers, we are able to reduce the order of the system [8].

4.2.1 SMC Example

An example is provided for better understanding the concept. A second order system is defined by the following equation;

$$m\ddot{x} + b\dot{x} + kx = u \tag{4.2}$$

The objective is the system to follow desired motion trajectory;

Objective $x \rightarrow x^d(x_{desired})$

The error is found by subtracting x^d from x;

$$e = x - x^d \tag{4.3}$$

The sliding function is chosen to be as following;

$$s = \dot{e} + \lambda e = \dot{x} - \dot{x^d} + \lambda(x - x^d) \tag{4.4}$$

suppose s=0 is maintained. Then

$$\dot{e} + \lambda e = 0; \tag{4.5}$$

which implies that $e \rightarrow 0$ asymptotically.

To achieve convergence to s=0, s and its derivative are enforced to have opposite signs, defines the following reaching condition:

$$\dot{s} = -\eta sgn(s) \tag{4.6}$$

Instead of using the sgn fuction, saturation function is used in simulation with upper limit (1) and lower limit (-1).

The control input is found by solving $\dot{s} = 0$ for u;

$$\dot{s} = \ddot{x} - \ddot{x^d} + \lambda(\dot{x} - \dot{x^d}) = -\eta sgn(s) \tag{4.7}$$

$$\frac{1}{m}(u - b\dot{x} - kx) = \ddot{x^d} - \eta sgn(s) - \lambda\dot{e} \tag{4.8}$$

$$u = \frac{1}{n}(-m\eta sgn(s) + m\ddot{x^d} - m\lambda\dot{x} - m\lambda\dot{x^d} + b\dot{x} + cx) \tag{4.9}$$

For the simulation; desired function is chosen as $sin(t)$ and the parameters are chosen as:

- m=1.7
- b=12
- k=1
- c=0
- n=1.25

The control gains λ, η, and ϕ were tuned in the simulation and decided as:

- $\lambda = 10$
- $\phi = 1$
- $\eta = 5$

The model of the example sytem is shown in Figure 4.3 and the result is shown in Figure 4.4. Also phase portrait is provided in Figure 4.5 and SMC function surface is shown in Figure 4.6.

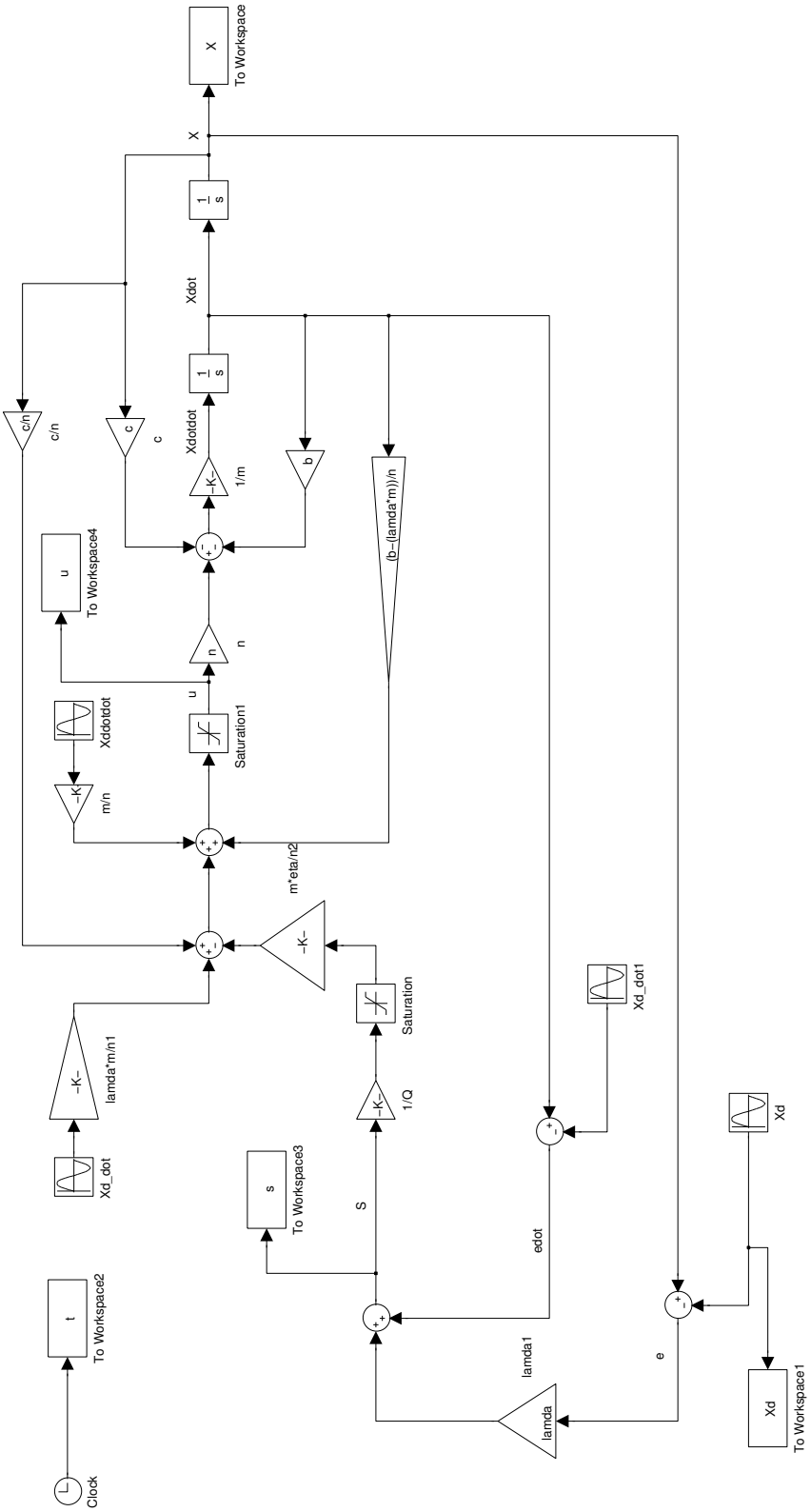

Figure 4.3: Sliding Mode Example

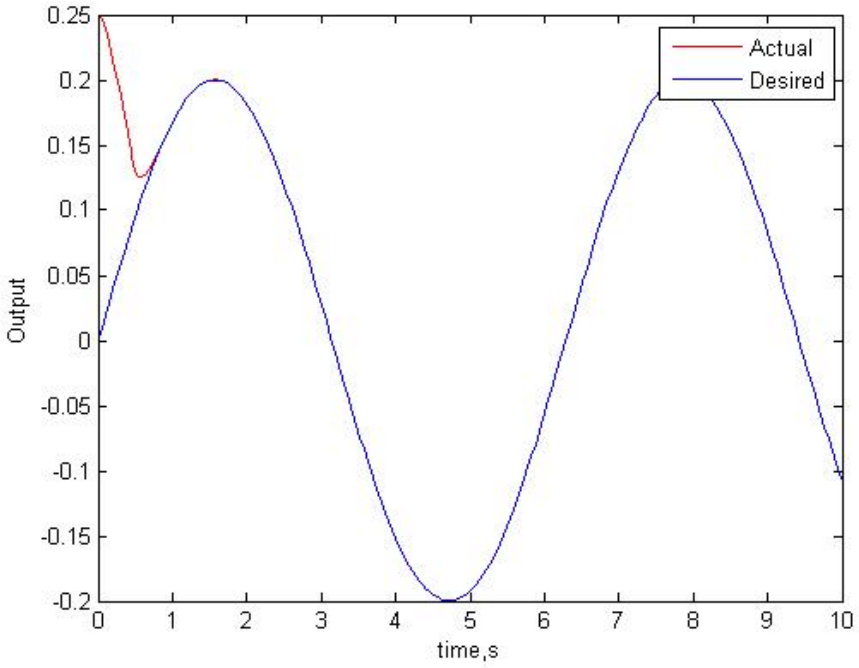

Figure 4.4: SMC example output

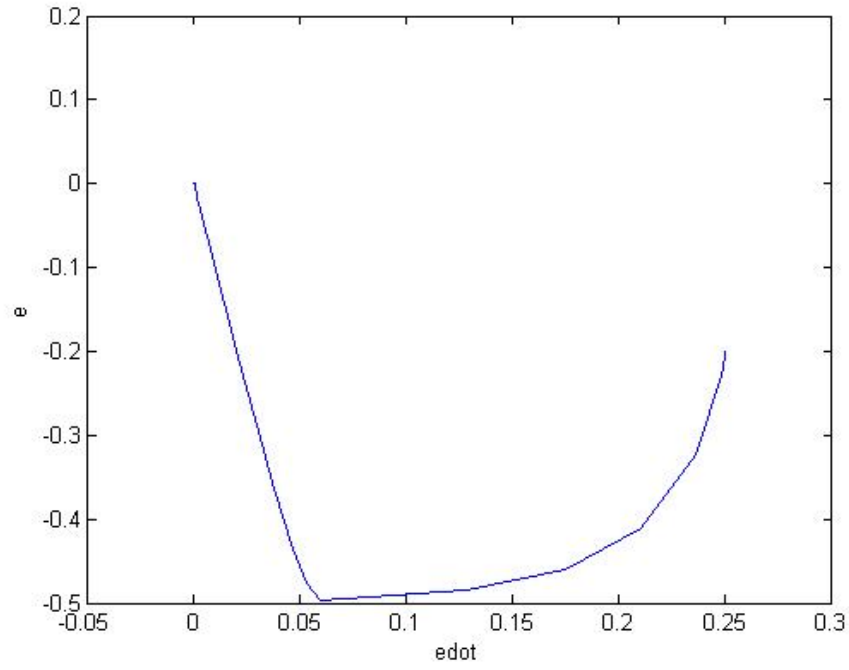

Figure 4.5: SMC phase protrait of the system

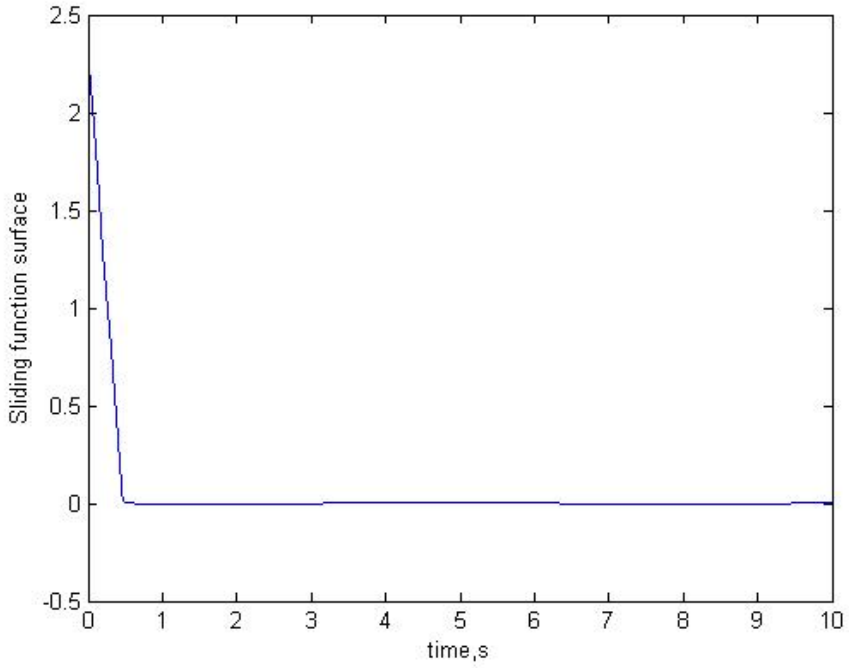

Figure 4.6: SMC function surface

4.3 Sliding Mode Velocity Control of the Treadmill

The symbolic equation of the system is solved to find the input used in the sliding mode control simulation. The same steps are applied to to find input as it is described in section 4.2.1.

$m\ddot{x} + b\dot{x} + cx = nu$

where x represents belt velocity and u is input voltage.

Objective $x \rightarrow x^d(x_{desired})$

$e = x - x^d$

Sliding function surface=s=$\dot{e} + \lambda e = \dot{x} - \dot{x^d} + \lambda(x - x^d)$

Reaching condition= $\dot{s} = -\eta sgn(s)$

$$\dot{s} = \ddot{e} + \lambda\dot{e} = \ddot{x} - \ddot{x^d} + \lambda(\dot{x} - \dot{x^d}) = \eta sgn(s)$$

$$\ddot{x} = \frac{n}{m}u - \frac{b}{m}\dot{x} - \frac{c}{m}x$$

$$\ddot{x} = -\eta sgn(s) + \ddot{x^d} - \lambda\dot{x} + \lambda\dot{x^d}$$

$$u = \frac{1}{n}(m(-\eta sgn(s) + \ddot{x^d} - \lambda\dot{x} + \lambda\dot{x^d}) + b\dot{x} + cx)$$

$$u = \frac{1}{n}(-m\eta sgn(s) + m\ddot{x^d} - m\lambda\dot{x} - m\lambda\dot{x^d} + b\dot{x} + cx)$$

4.3.1 Observer Design

For a feedback system design, all states might not be available for feedback in a real-time experiment. Additional sensors would be required to measure all states and make them available for feedback. However, when the number of sensors is increased, the cost would increase and also the system would be more complex. The states that are not directly measured can be estimated when the sytem is observable. A full-state observer for a system with equations $\dot{x} = Ax + Bu$, and $y = Cx + Du$ is defined as:

$$\dot{\hat{x}} = A\hat{x} + Bu + L(y - C\hat{x}) \tag{4.10}$$

where $\hat{x}$ indicates estimation of the state x. L is the observer gain matrix that will be discussed later.

The observer estimation error is calculated as:

$$e(t) = x(t) - \hat{x}(t) \tag{4.11}$$

By taking the time derivative of the error and implementing the observer, the following equation is obtained:

$$\dot{e}(t) = (A - LC)e(t) \tag{4.12}$$

L is found by defining the characteristic equation. For a second order system it can be defined as following:

$$det(\lambda I - (A - LC)) = {}^2 + 2\zeta\omega_n\lambda + {\omega_n}^2 \tag{4.13}$$

where ζ and ω_n are selected according to desired setling time.

4.3.2 Observer Design for the System

For real time experiment of our system, the acceleration cannot be measured. In order to have this state it is needed to design an observer. First of all the state-space representation of TF Eq (4.14) is:

$$m\ddot{x} + b\dot{x} + cx = nu \tag{4.14}$$

where x represents belt velocity and u is input voltage.

$x_1 = x$

$x_2 = \dot{x}$

$\dot{x_1} = x_2$

$\dot{x_2} = \frac{n}{m}u - \frac{b}{m}x_2 - \frac{c}{m}x_1$

$y = x_1$

$$A = \begin{bmatrix} 0 & 1 \\ -\frac{c}{m} & -\frac{b}{m} \end{bmatrix}$$

$$B = \begin{bmatrix} 0 \\ -\frac{n}{m} \end{bmatrix}$$

$$C = \begin{bmatrix} 1 & 0 \end{bmatrix}$$

$$D = \begin{bmatrix} 0 \end{bmatrix}$$

where $m = 5$, $b = 24.14$, and $c = 174.9$

For the next step, the observability of the system is checked. Since $\det(P_o) = 1 \neq 0$, the system is observable.

$$P_o = \begin{bmatrix} C \\ CA \end{bmatrix}$$

The L matrix is found by equating the coefficients in the equation:

$det(\lambda I - (A - LC)) = \lambda^2 + 2\zeta\omega_n + {\omega_n}^2$

where ζ and ω_n are chosen 0.8 and 10 respectively to have settling time less than 0.5 seconds.

$L_1 = -8.14$

$L_2 = -1043.9$

The model of the system is shown in Figure 4.7. The results are shown Figures 4.8 and 4.9. As a conclusion, observer design provided a good estimation of the states that will be used in the real system.

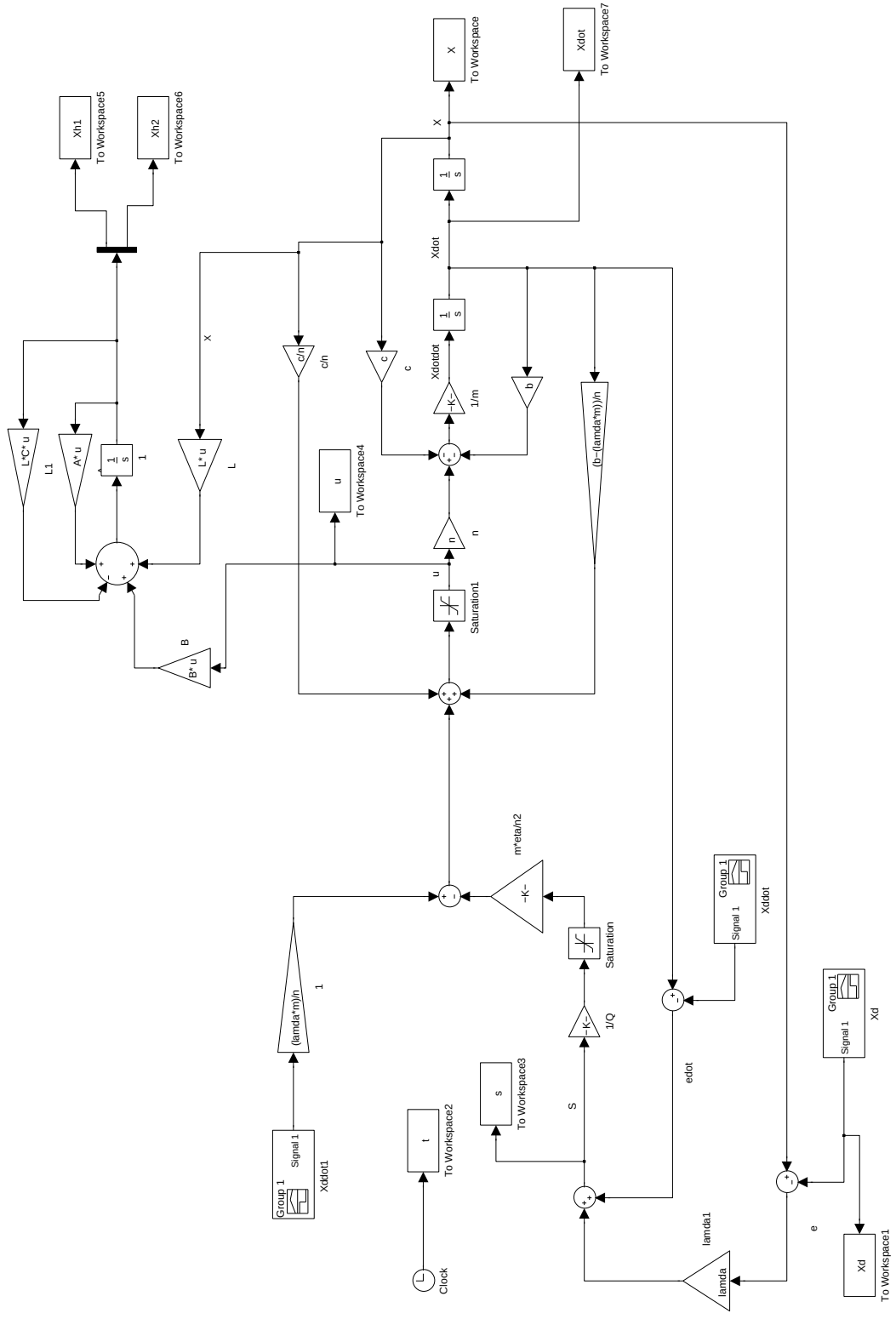

Figure 4.7: Model of the system with SMC

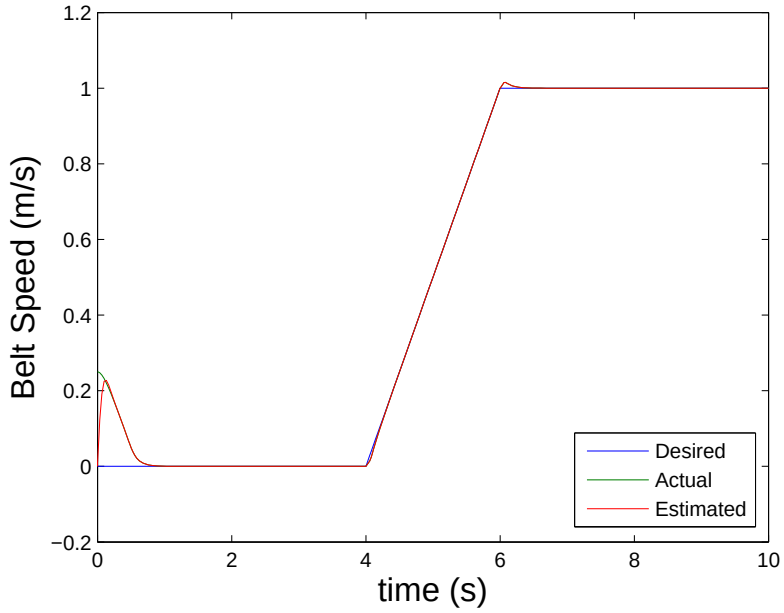

Figure 4.8: Velocity output of the model with ramp input

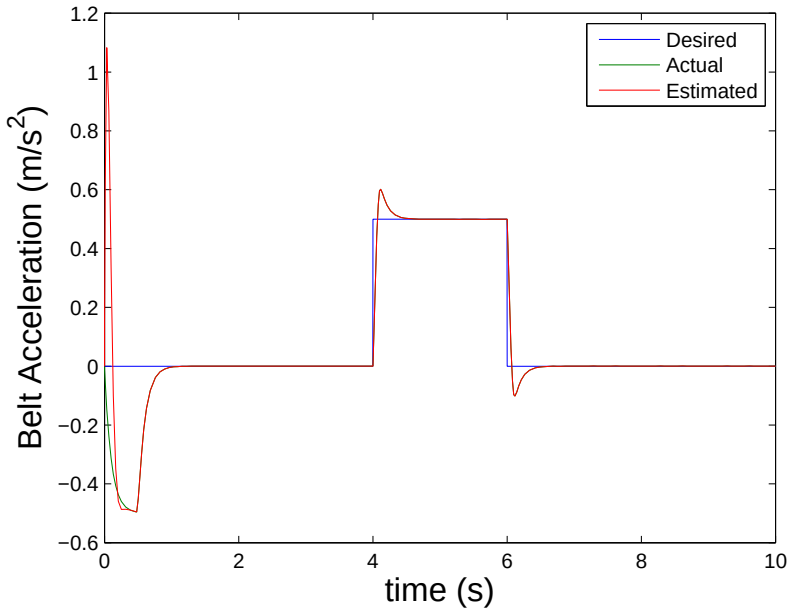

Figure 4.9: Acceleration output of the system with ramp input

CHAPTER V

REAL TIME EXPERIMENTS

Real time experiments involving accelerations, decelerations, constant speeds and sinusoidal movement of the belt are conducted. Tests were also conducted with a subject and a prosthesis attached to a robotic hip simulator. In addition, alternative conditions such as waved and backward walking are provided.

5.1 Constant Speed Tests

Commercial treadmills operate at constant speed. The PID and SMC controllers were implemented in the system under controlled constant speed. Tests are conducted while a human subject is walking and running at different speeds. The results of the two controllers and the original controller built into the treadmill are compared.

5.1.1 Real Time Interface

For PID and SMC, a step input is fed into each system to test control performance. For the original controller, the output is recorded. Figures 5.1, 5.2 and 5.3 show the real-time interfaces used for the original controller, the PID controller and the SMC, respectively.

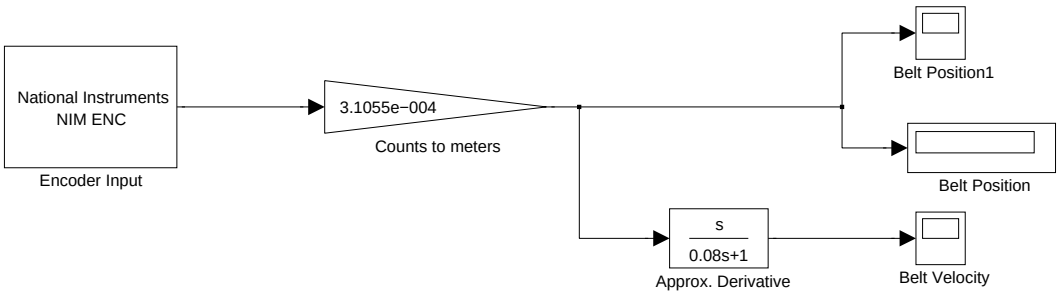

Figure 5.1: Interface for system with original controller

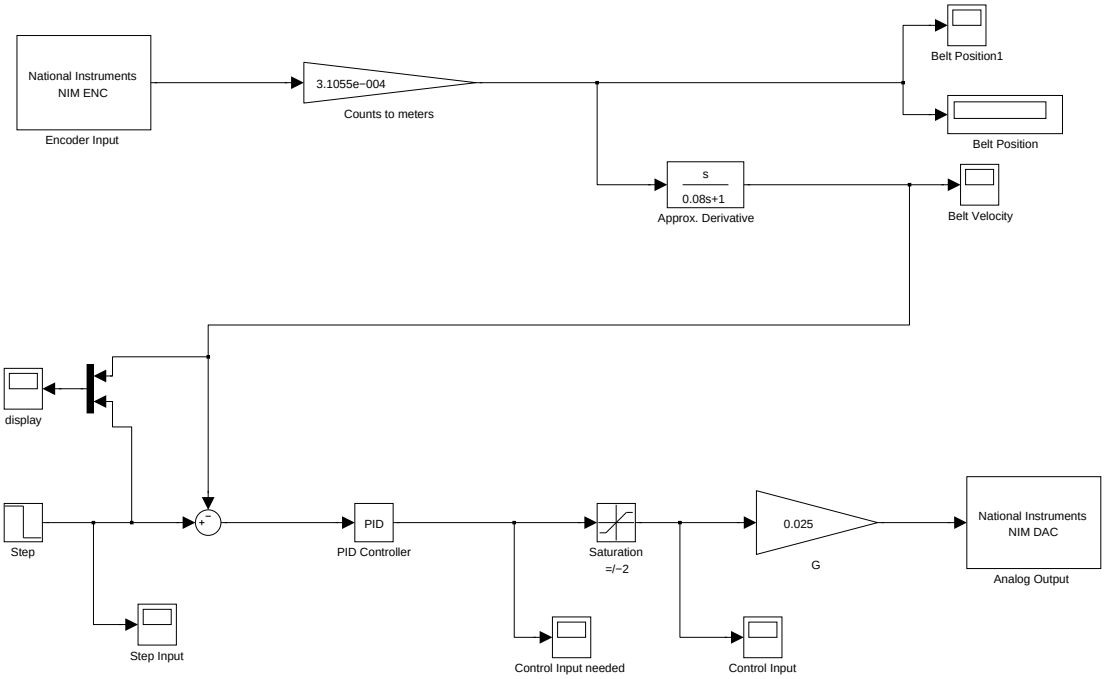

Figure 5.2: Interface for the system with PID controller

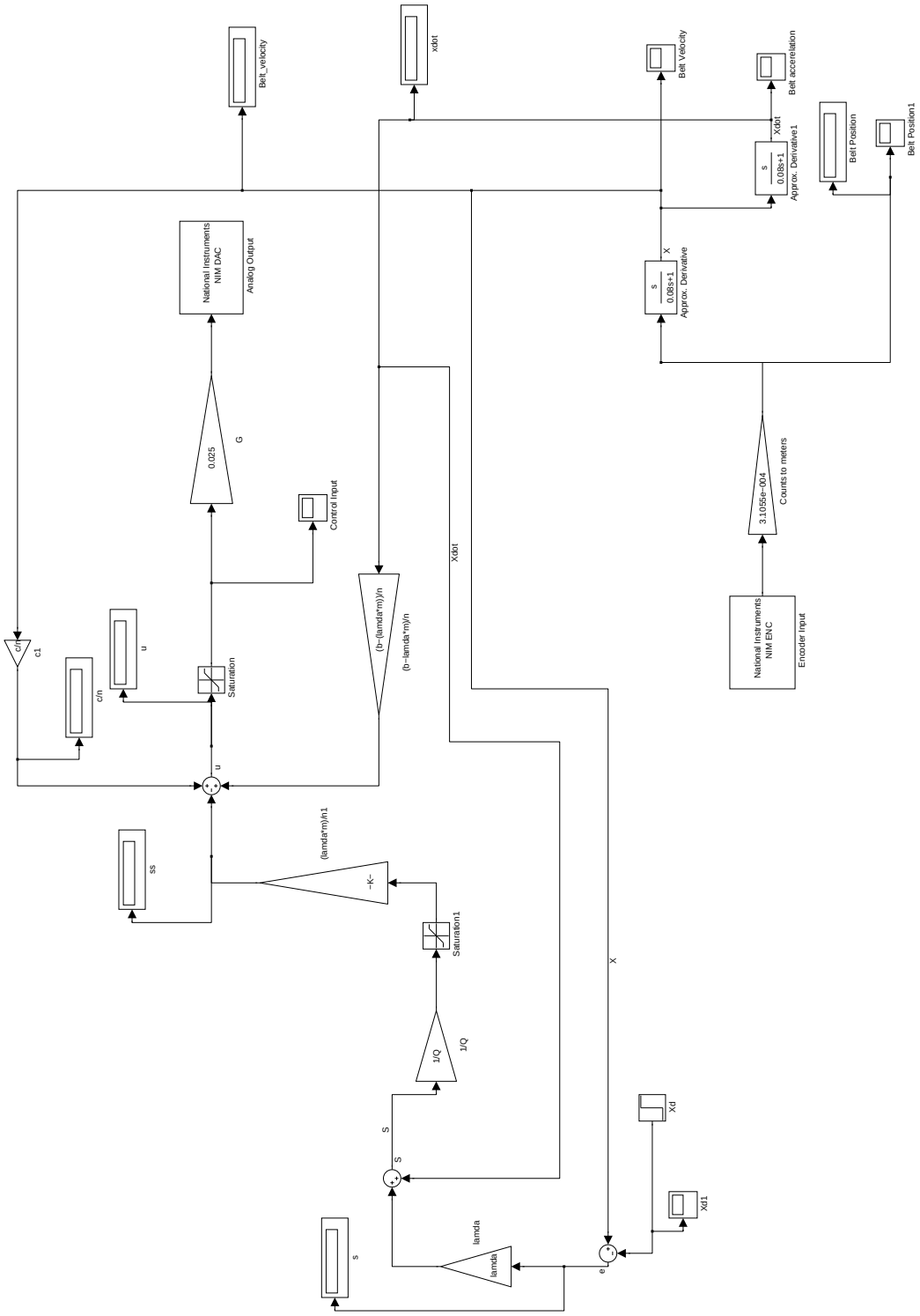

Figure 5.3: Interface for the system with SMC controller

5.1.2 Constant-speed Results

Different constant speed tests were conducted with a range between 1 mile/h (0.44 m/s) and 2.2 mile/h (0.98 m/s) due to power supply limitations. Tests are done in both directions, forward and backward. In one case with the subject walking backwards, only PID and the SMC controllers are compared, since the original controller does not have this option. PID gains are tuned as 300, 950, and 0 respectively. SMC gains are chosen as: $\lambda = 90$, $\eta = 160$, and $\phi = 0.8$. The original controller is also included for comparison while the subject is moving forward. Figures 5.4 and 5.7 show the test results with speeds of 1.3 mile/h (0.58 m/s) and 2.1 mile/h (0.93 m/s) with the subject moving backwards. Figures 5.5 and 5.5 show test results with speeds of 1.3 mile/h (0.58 m/s) and 2.1 mile/h (0.93 m/s) with the subject moving forward. The tests are conducted with a subject whose weight is 88 kg. The subject started to walk at the 4th second and stepped down at the 14th second. Both controllers showed good tracking under no-load conditions. However, when the subject was on treadmill, the responses were slightly different. With the PID controller, belt speed oscillated above and below the reference with each step. With SMC, belt speed was slightly lower than the reference during foot contact, but no overshoot was observed after each step. Both controllers were better than the original controller, which also had offset error.

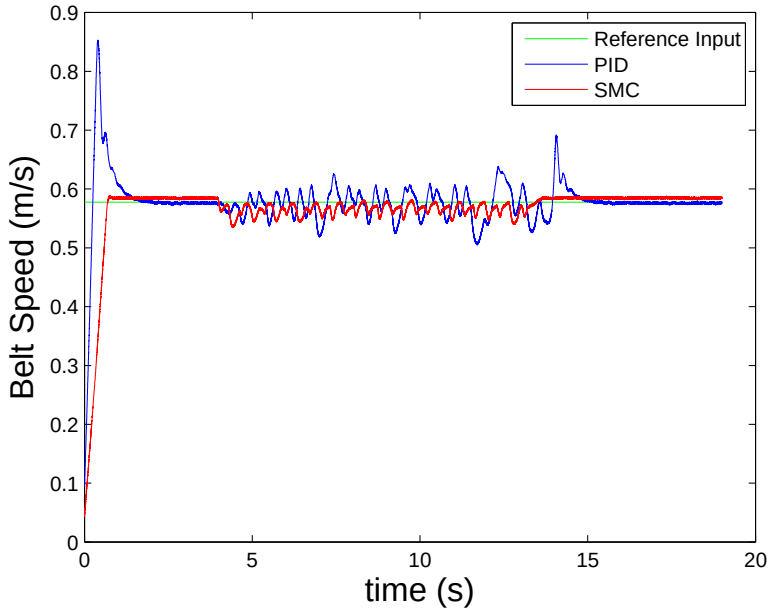

Figure 5.4: Constant speed test results with a speed of 1.3 mile/h with the subject moving backwards.

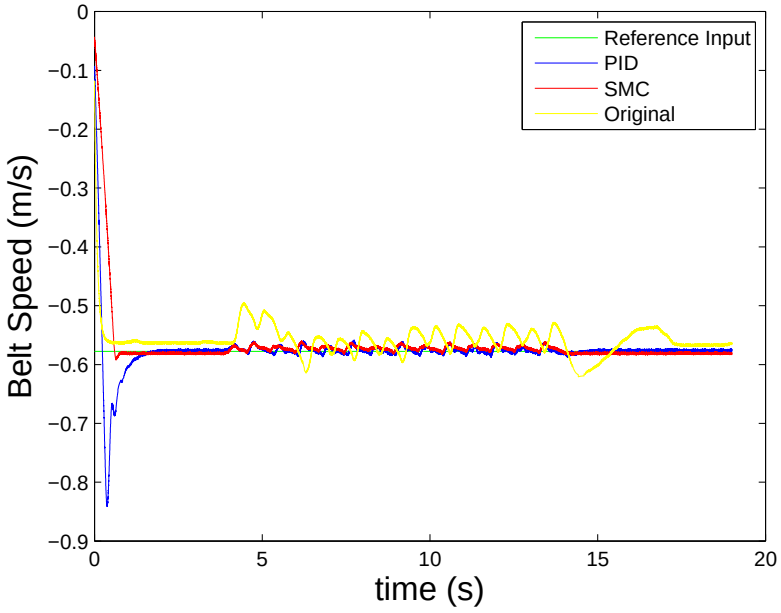

Figure 5.5: Constant speed test results with a speed of 1.3 mile/h with the subject moving forward.

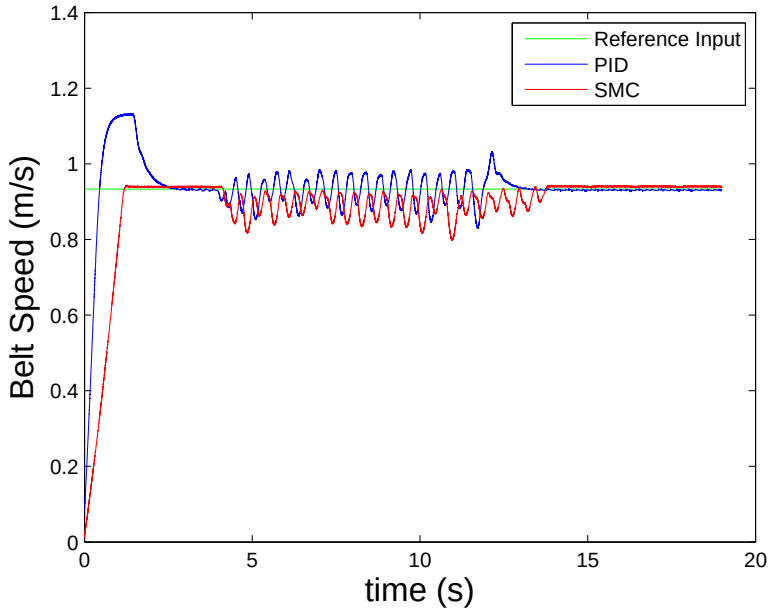

Figure 5.6: Constant speed test results with a speed of 2.1 mile/h with the subject moving backwards.

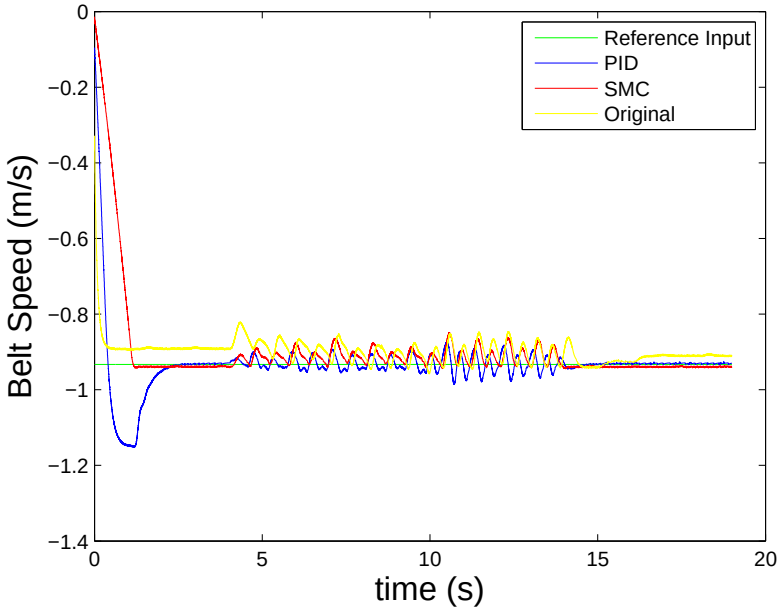

Figure 5.7: Constant speed test results with a speed of 2.1 mile/h with the subject moving forward.

Voltage limitations were the main obstacle to the achievement of higher tracking accuracy. At lower speeds, the supplied voltages were sufficient; however, with the required voltage exceeded saturation limits for higher speeds. In the models, the saturation block is used to bound control voltage between 40 V and -40 V which are the limits of the power amplifier. In addition, the required voltage while subject was moving backwards was more than the voltage while subject was moving backwards when foot contact. It is concluded that the subject applied more force on the treadmill while moving backwards. Figures 5.8 and 5.12 show the required and supplied control voltages for the PID controller and Figures 5.9 and 5.13 show the voltages for the SMC controller with the subject moving backwards. Figures 5.10 and 5.14 show the required and supplied control voltages for the PID controller and Figures 5.11 and 5.15 show the voltages for the SMC controller with the subject moving forward.

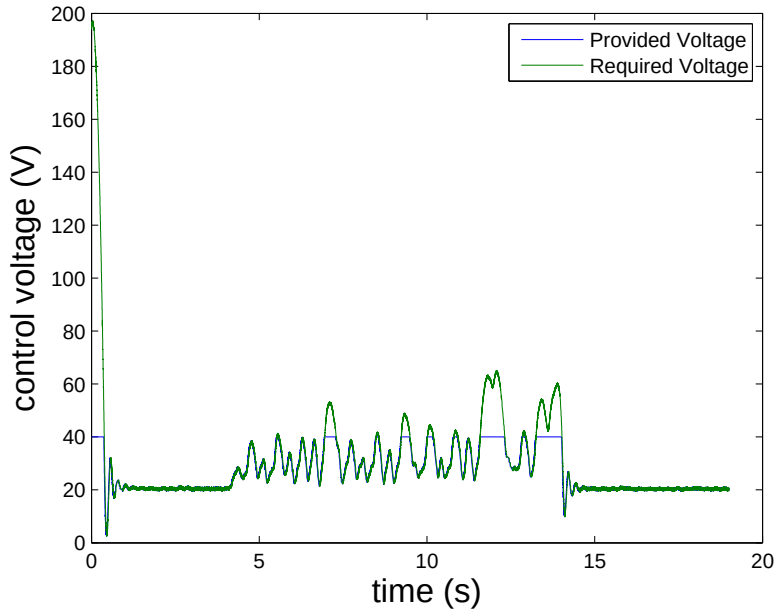

Figure 5.8: Controller voltage at a speed of 1.3 mile/h for the PID with the subject moving backwards

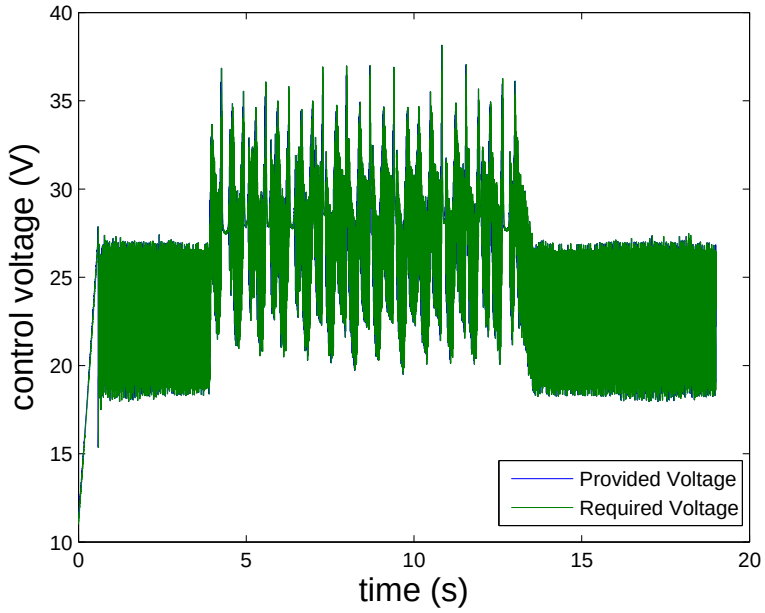

Figure 5.9: Controller voltage at a speed of 1.3 mile/h for the SMC with the subject moving backwards

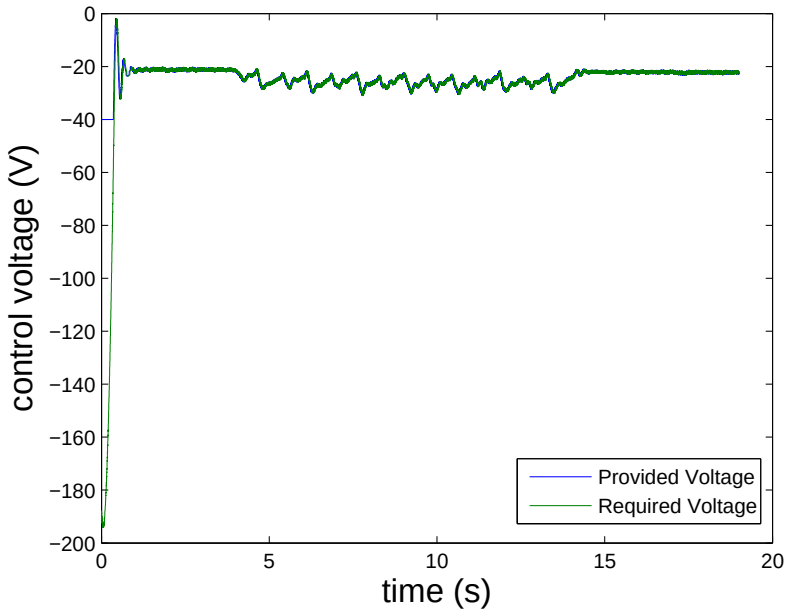

Figure 5.10: Controller voltage at a speed of 1.3 mile/h for the PID with the subject moving forward.

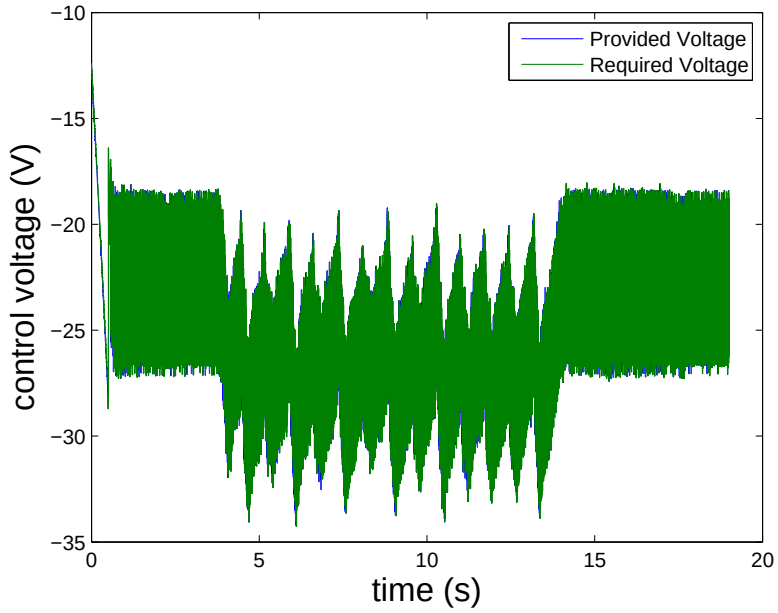

Figure 5.11: Controller voltage at a speed of 1.3 mile/h for the SMC with the subject moving forward.

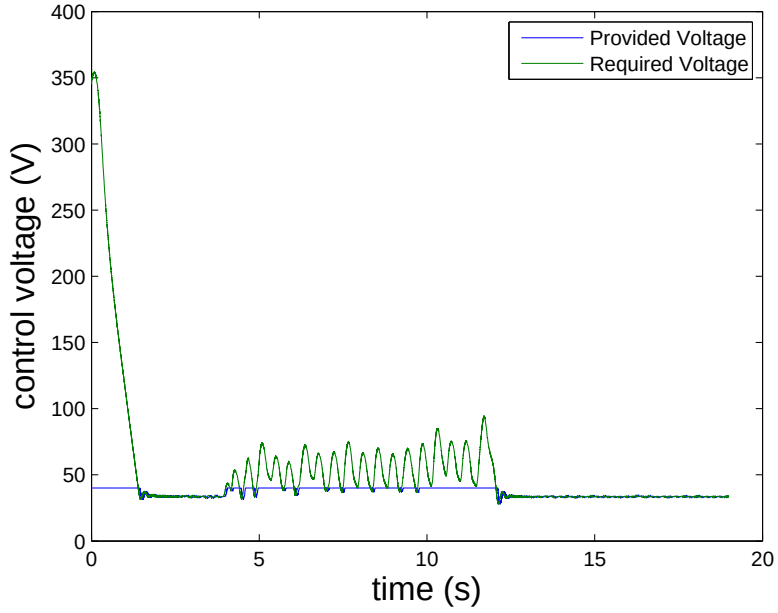

Figure 5.12: Controller voltage at a speed of 2.1 mile/h for the PID with the subject moving backwards

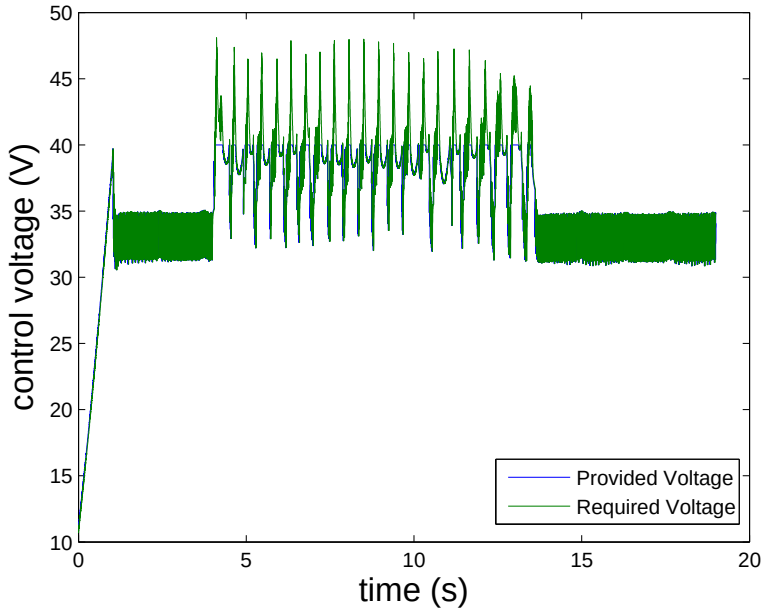

Figure 5.13: Controller voltage at a speed of 2.1 mile/h for the SMC with the subject moving backwards

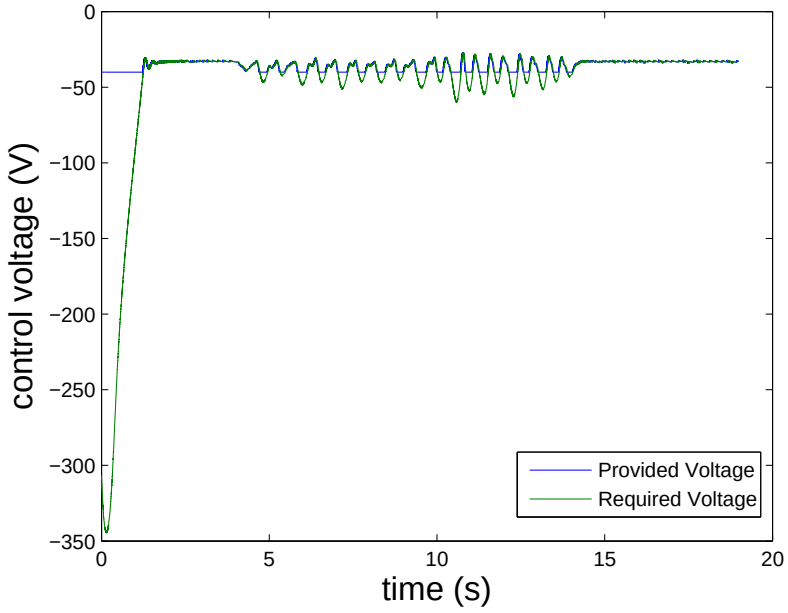

Figure 5.14: Controller voltage at a speed of 2.1 mile/h for the PID with the subject moving forward.

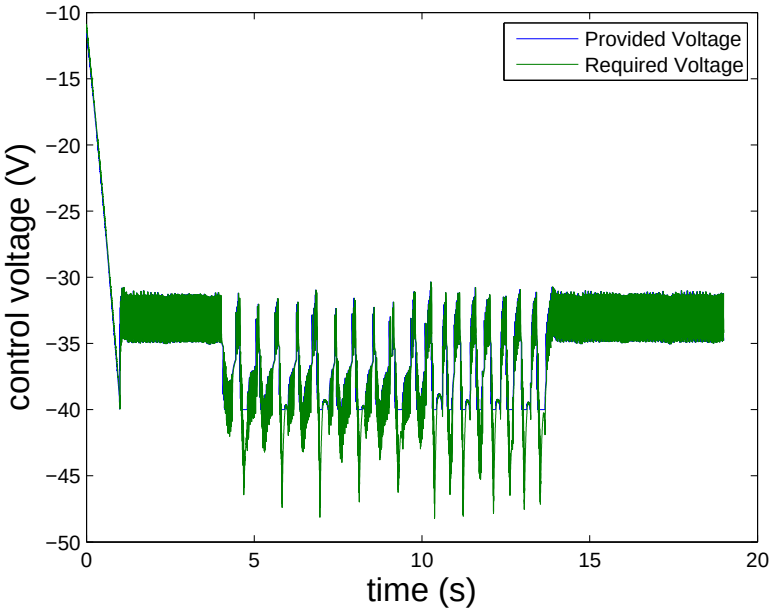

Figure 5.15: Controller voltage at a speed of 2.1 mile/h for the SMC with the subject moving forward.

5.2 Acceleration and Deceleration Tests

Acceleration and deceleration are involved in normal walking and running activities. Traditional treadmills are not capable of simulate these movements, since they are generally used for training in a constant speed mode. In this section a PID controller and sliding mode controller are fed by a ramp input with different slopes. The results of the two controllers are compared.

5.2.1 Results

The acceleration and deceleration test are done along both directions, forward and backward. The experiments were conducted with a subject whose weight is 88 kg. The highest slope used was 0.9 m/s^2 due to power restrictions. PID gains are tuned as 600, 950, and 0 respectively. SMC gains are chosen as: $\lambda = 10$, $\eta = 70$, and

$\phi = 0.5$. PID and SMC showed similar results in both directions. Figures 5.16, 5.17, and 5.18 show the test results with slopes of 0.3 m/s^2, 0.45 m/s^2, and 0.9 m/s^2 respectively, with the subject moving backwards. Only one leg is used due to the fact that it was diffucult for subject to maintain balance. Figures 5.19, 5.20, and 5.21 show the test results with slopes of 0.3 m/s^2, 0.45 m/s^2, and 0.9 m/s^2, respectively, with the subject moving forward. Both legs were used in this test. Both controllers provided good tracking with low slopes; however, the SMC showed better tracking when the slope increased.

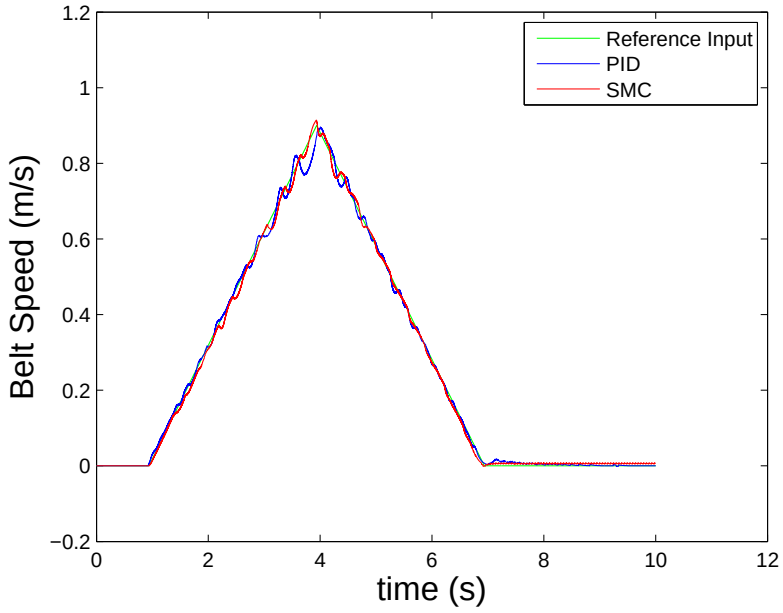

Figure 5.16: Acceleration and deceleration test results with slope of 0.3 m/s^2 , with the subject moving backwards.

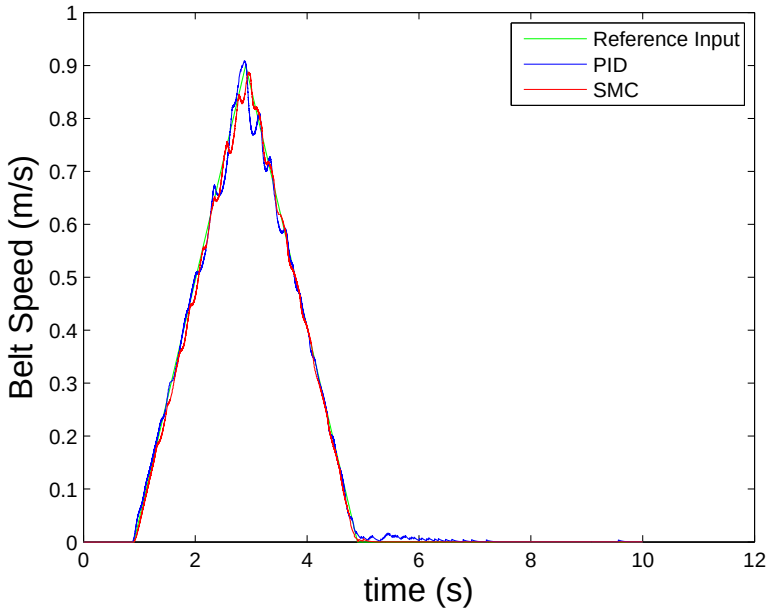

Figure 5.17: Acceleration and deceleration test results with slope of 0.45 m/s^2, with the subject moving backwards.

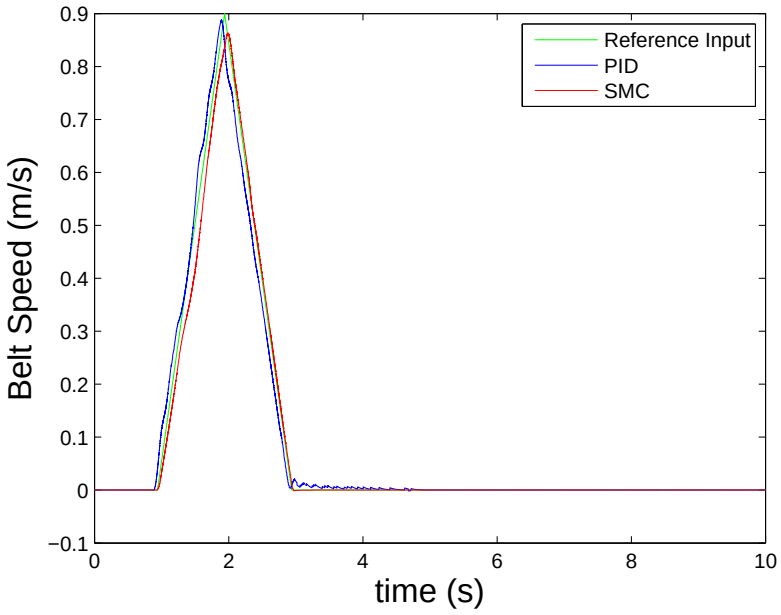

Figure 5.18: Acceleration and deceleration test results with slope of 0.9 m/s^2, with the subject moving backwards.

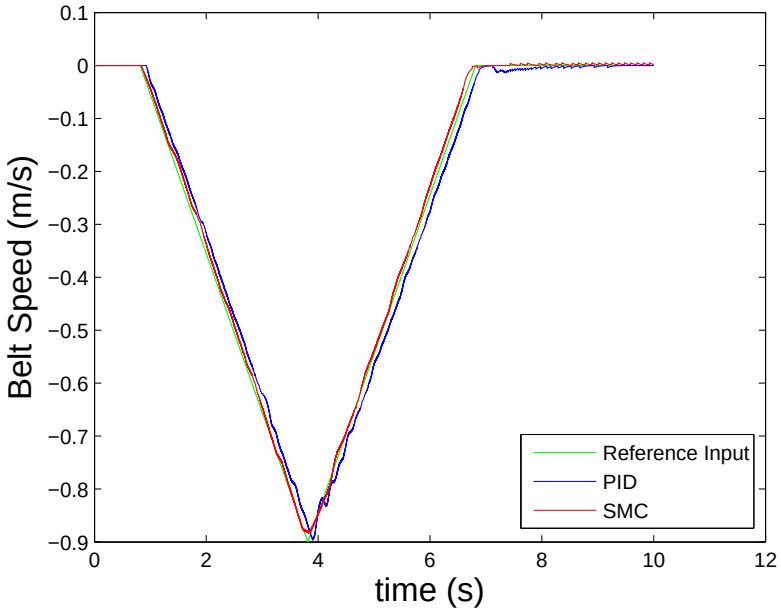

Figure 5.19: Acceleration and deceleration test results with slope of 0.3 m/s^2 , with the subject moving forward.

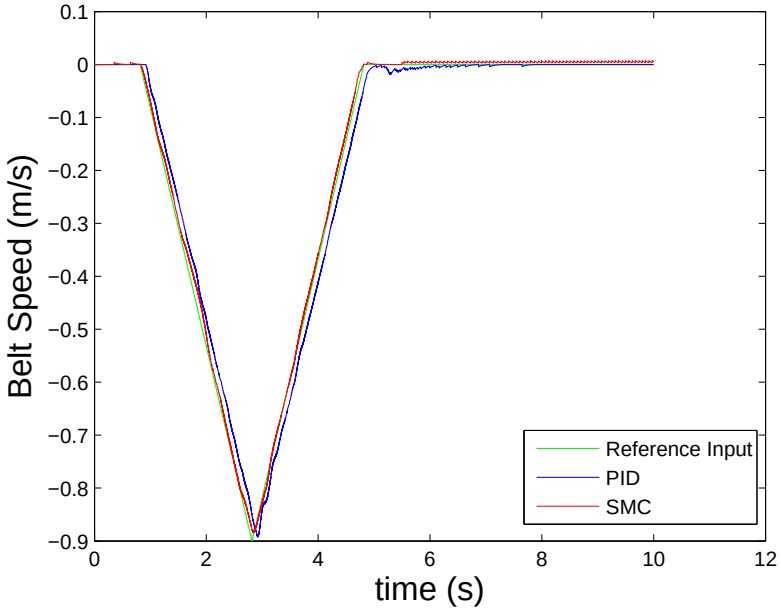

Figure 5.20: Acceleration and deceleration test resultswith slope of 0.45 m/s^2, with the subject moving forward.

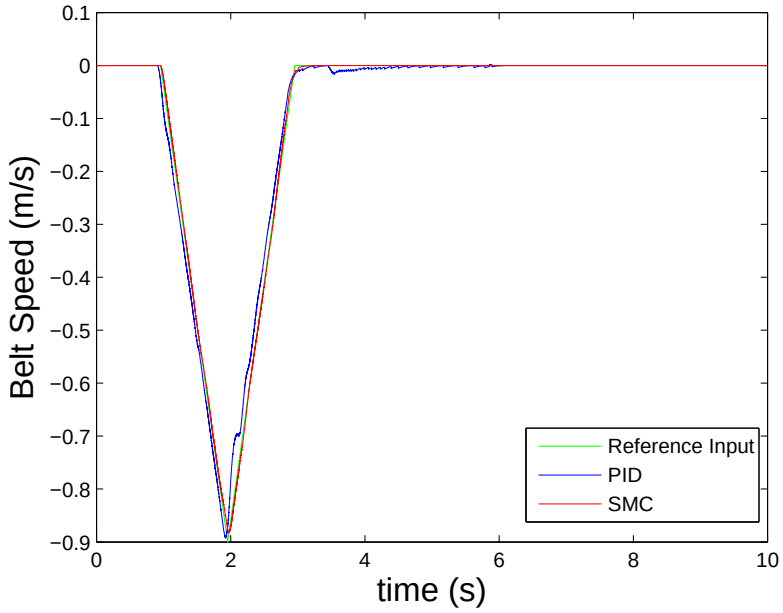

Figure 5.21: Acceleration and deceleration test results with slope of 0.9 m/s^2, with the subject moving forward.

5.3 Tests with Different Walking Conditions

People confront many different factors such as wind that affect their walking experience outdoors. Also, specific walking patterns are needed for rehabilitation purposes. In this section, various tests are conducted to simulate the situations described above.

5.3.1 Simulating Windy Weather

With implementing a controller into treadmill system, different walkways can be simulated by changing the reference input. The signal builder block available in the real-time interface was used to create a biased sinewave. Both PID and SMC controller showed good results. Forward and backward directions were used. PID gains were tuned as 300, 950, and 0 respectively. SMC gains were chosen as: $\lambda = 90$, $\eta = 160$, and $\phi = 0.8$. Frequency was kept under 12 Hertz due to power amplifier

restrictions.

Results

The test are conducted by same person whose weight is 88 kg. The step input was used to provide a bias to the sinewave, and it was always 0.7 m/s. For the sinusoidal signal, the amplitude was always 0.1 m/s and the frequencies changed from 5 Hz to 12 Hz. Both controllers showed good tracking.

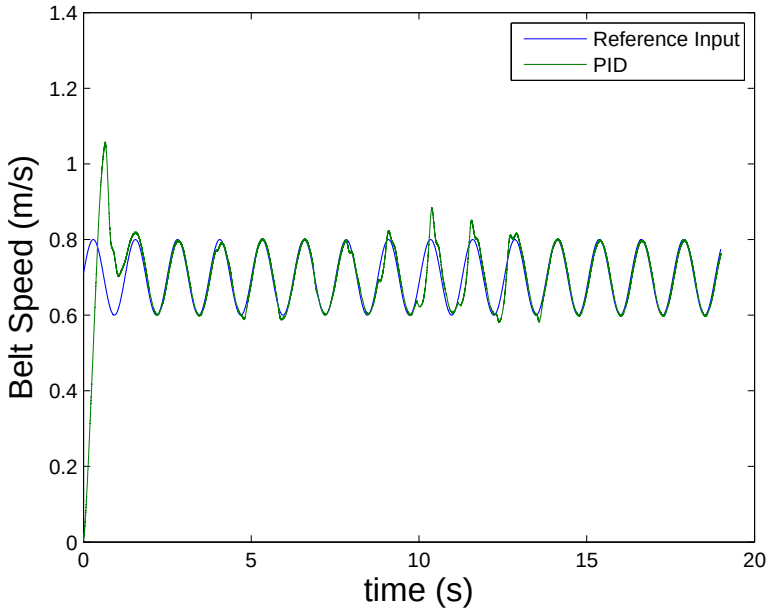

Figure 5.22: Test results at 5 Hz with PID, with the subject moving backwards.

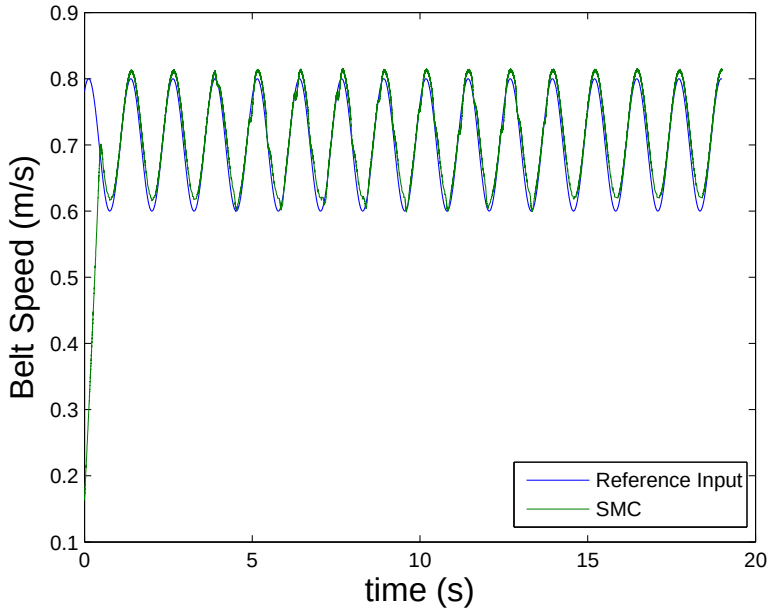

Figure 5.23: Test results at 5 Hz with SMC, with the subject moving backwards.

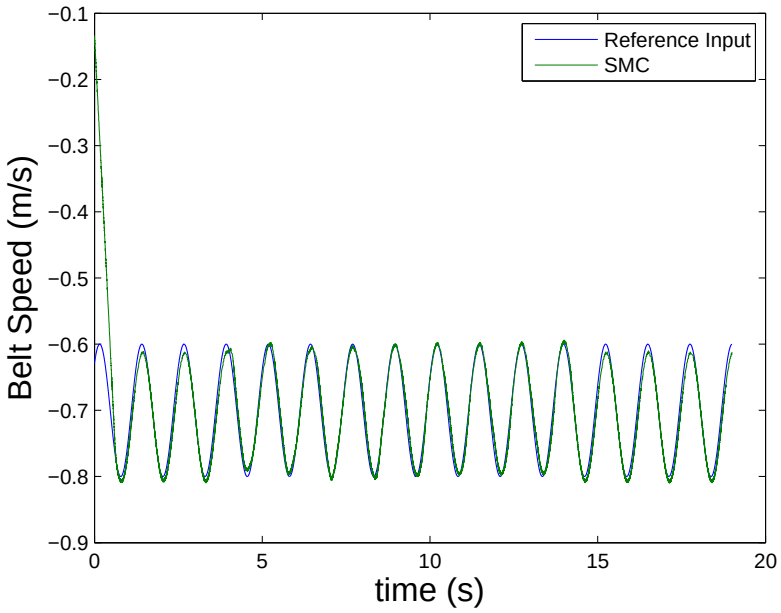

Figure 5.24: Test results at 5 Hz with PID, with the subject moving forward.

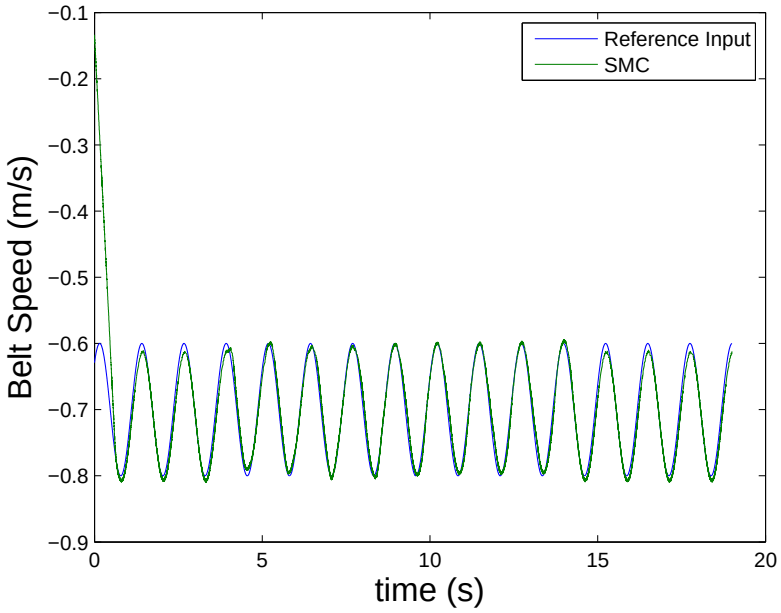

Figure 5.25: Test results at 5 Hz with SMC, with the subject moving forward.

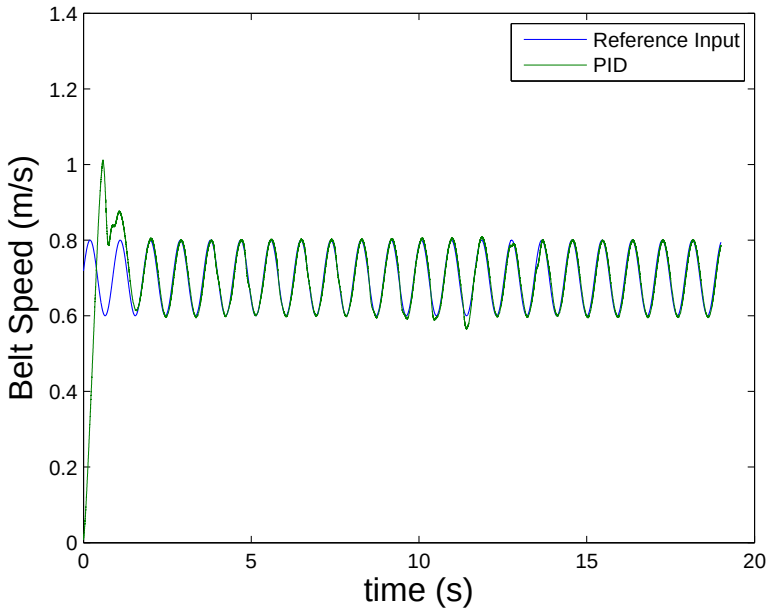

Figure 5.26: Test results at 7 Hz with PID, with the subject moving backwards.

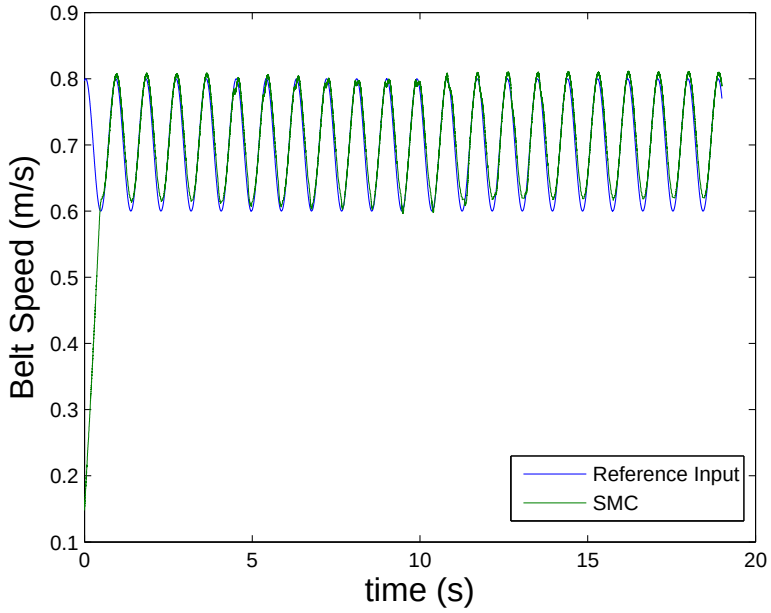

Figure 5.27: Test results at 7 Hz with SMC, with the subject moving backwards.

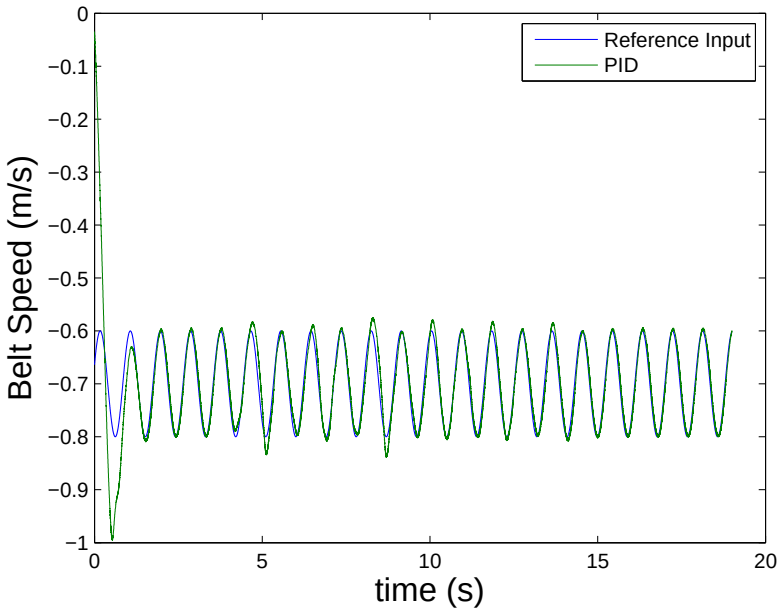

Figure 5.28: Test results at 7 Hz with PID, with the subject moving forward.

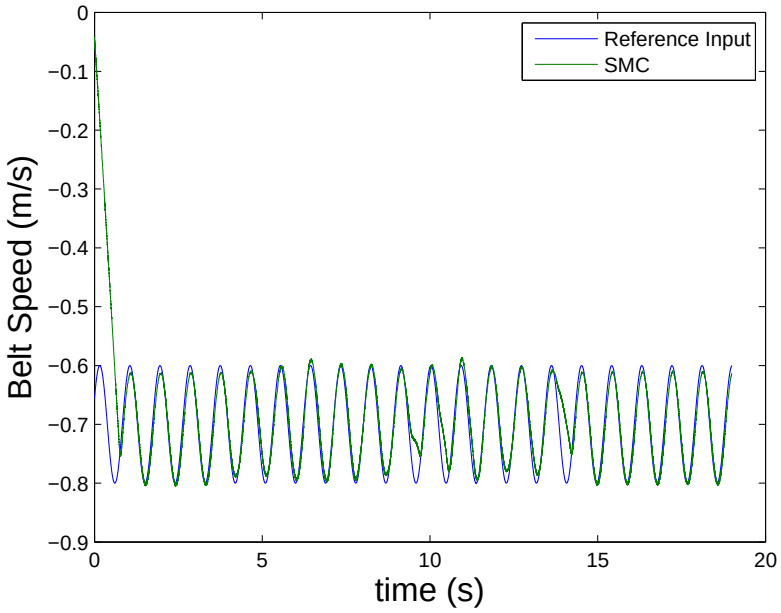

Figure 5.29: Test results at 7 Hz with SMC, with the subject moving forward.

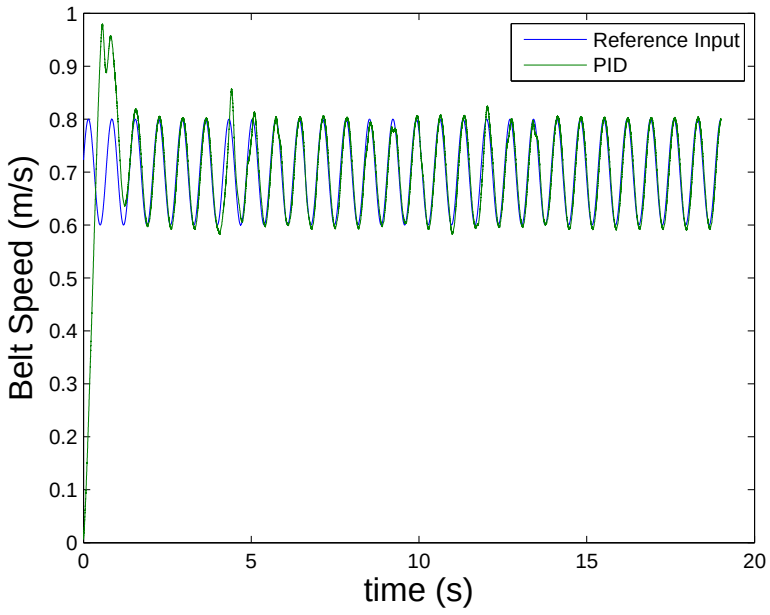

Figure 5.30: Test results at 9 Hz with PID, with the subject moving backwards.

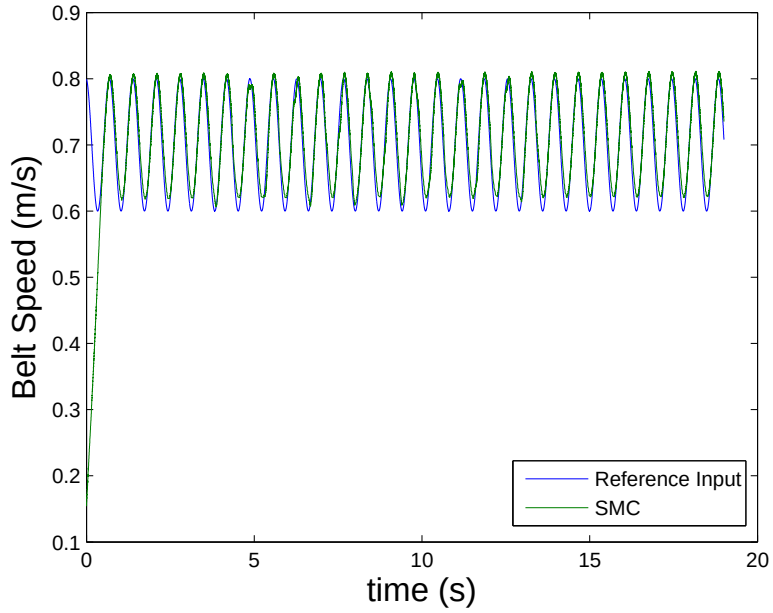

Figure 5.31: Test results at 9 Hz with SMC, with the subject moving backwards.

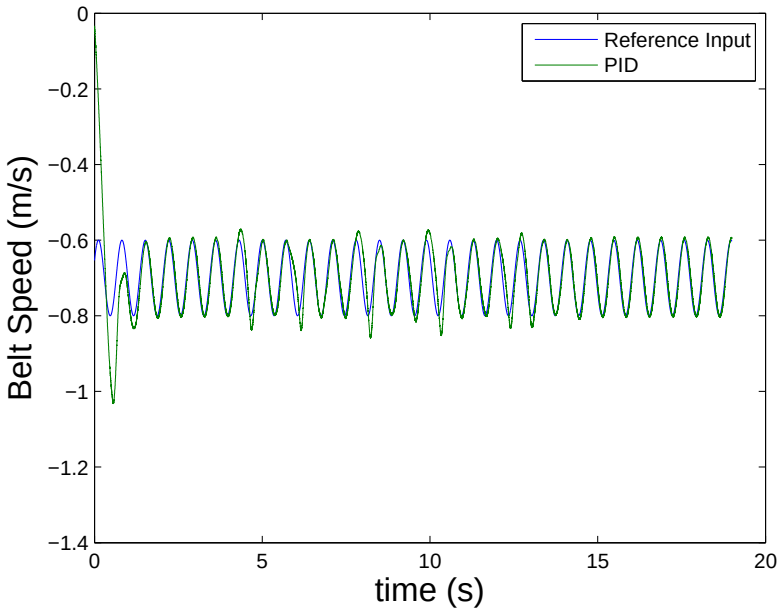

Figure 5.32: Test results at 9 Hz with PID, with the subject moving forward.

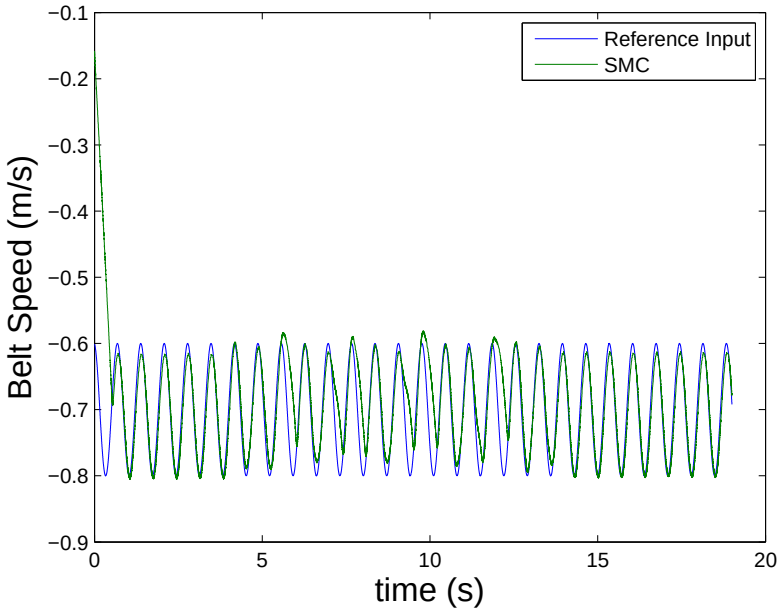

Figure 5.33: Test results at 9 Hz with SMC, with the subject moving forward.

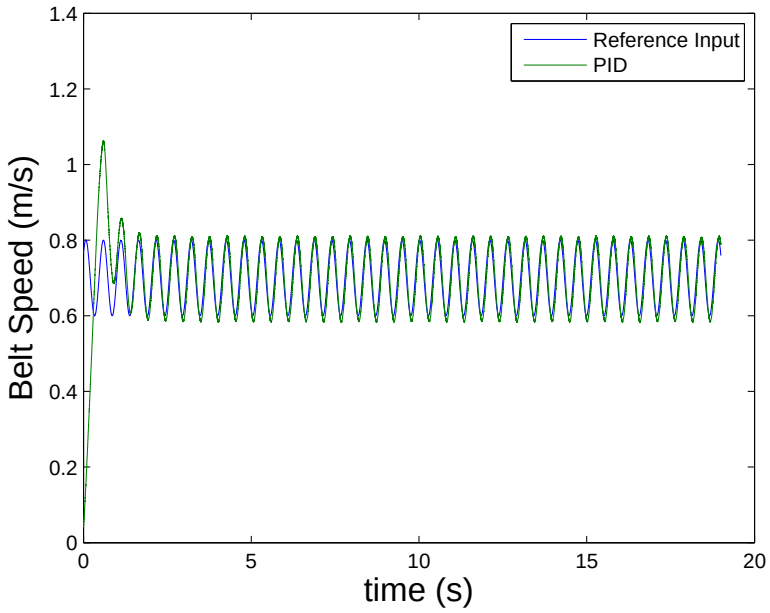

Figure 5.34: Test results at 12 Hz with PID, with the subject moving backwards.

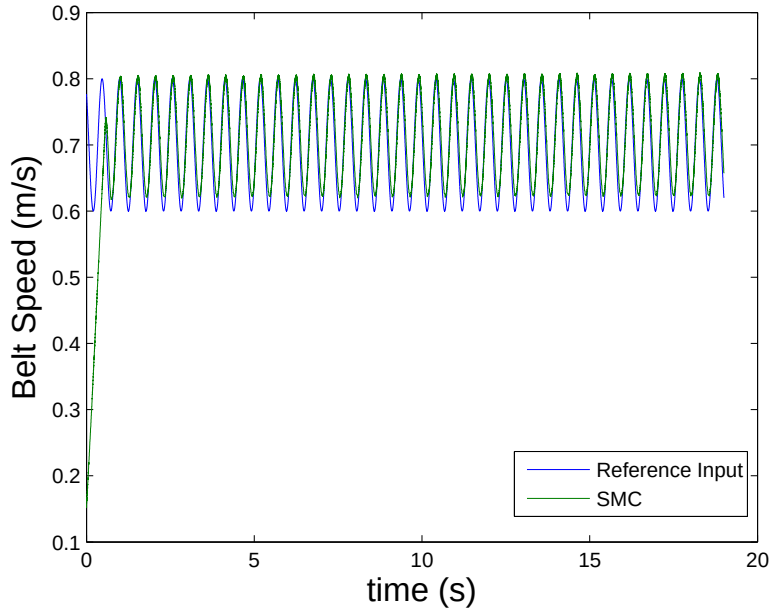

Figure 5.35: Test results at 12 Hz with SMC, with the subject moving backwards.

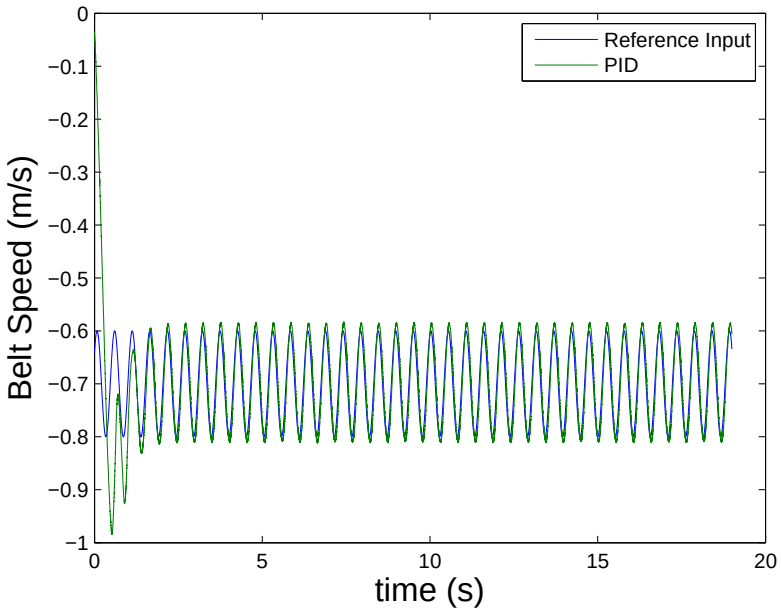

Figure 5.36: Test resultsat 12 Hz with PID, with the subject moving forward.

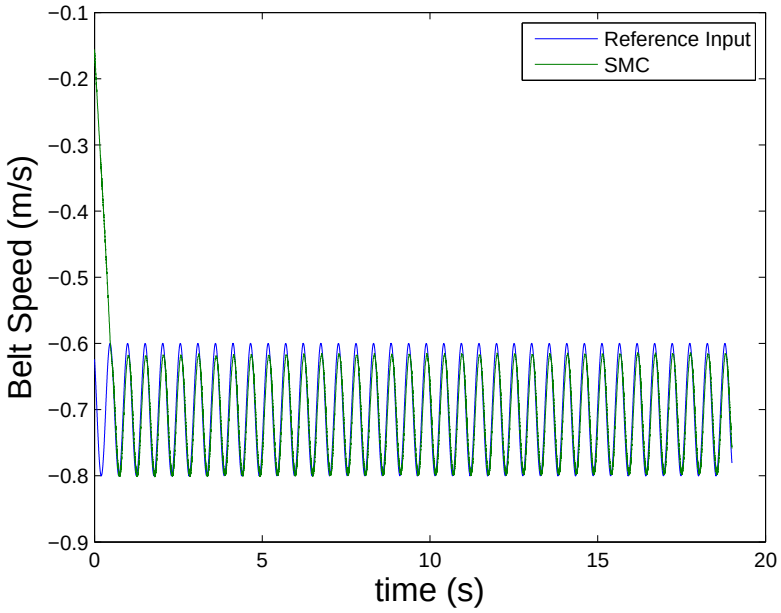

Figure 5.37: Test results at 12 Hz with SMC, with the subject moving forward.

5.3.2 Low Speed Tests

The treadmill available in the lab has a lowest selectable speed of 1 mile/hour (0.447 m/s). Lower speeds may be necessary for rehabilitation purposes. Step inputs from 0.05 m/s to 0.4m/s were fed into system. PID gains are tuned as 300, 950, and 0 respectively. SMC gains are chosen as: $\lambda = 75$, $\eta = 300$, and $\phi = 5$.

Results

The subject started walking at the 4th second and stepped down at 14th second. The performance with disturbance and without disturbance can be seen in the figures. Figure 5.38 show the results with speeds of 0.05 m/s, 0.1 m/s, 0.15 m/s, and 0.2 m/s with the subject moving forward, and Figure 5.38 show results with speeds of 0.25 m/s, 0.3 m/s, 0.35 m/s, and 0.4 m/s with the subject moving forward. The performance of both controllers were good because of the fact that the amplifier did not reach saturation.

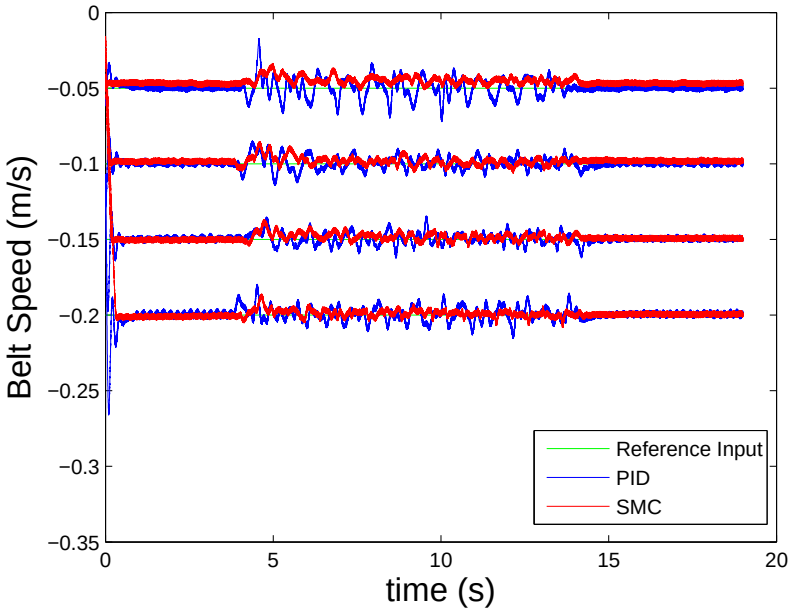

Figure 5.38: Low speed tests with the subject moving forward.

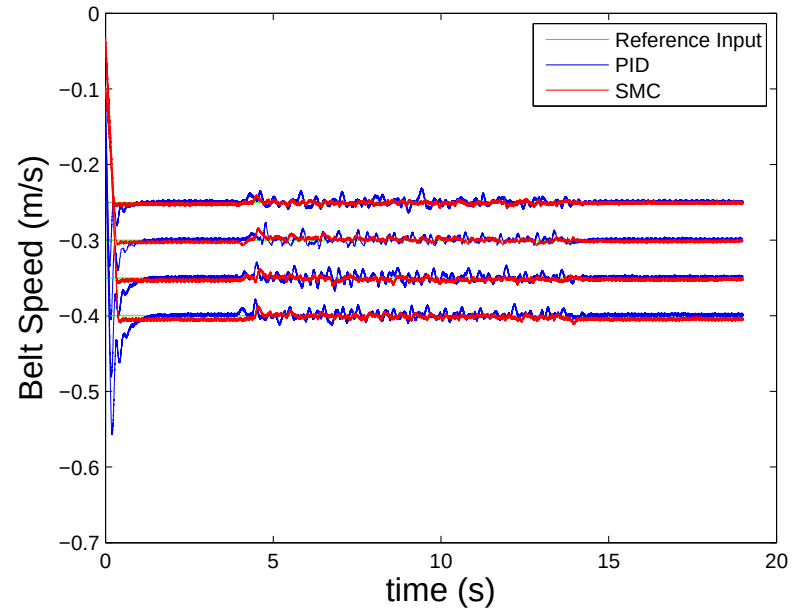

Figure 5.39: Low speed tests with the subject moving forward

5.3.3 Position Control

Belt position control is desired for specialized studies involving prosthetic leap and a robotic hip simulator. An obstacle can be mounted on the belt, which can be driven to a desired position. Only PID controller performance is tested in this experiment because of the fact that a new controller design was required for SMC. PID gains are tuned as 200, 1, and 0 respectively. The interface of the system shown in Figure 5.40.

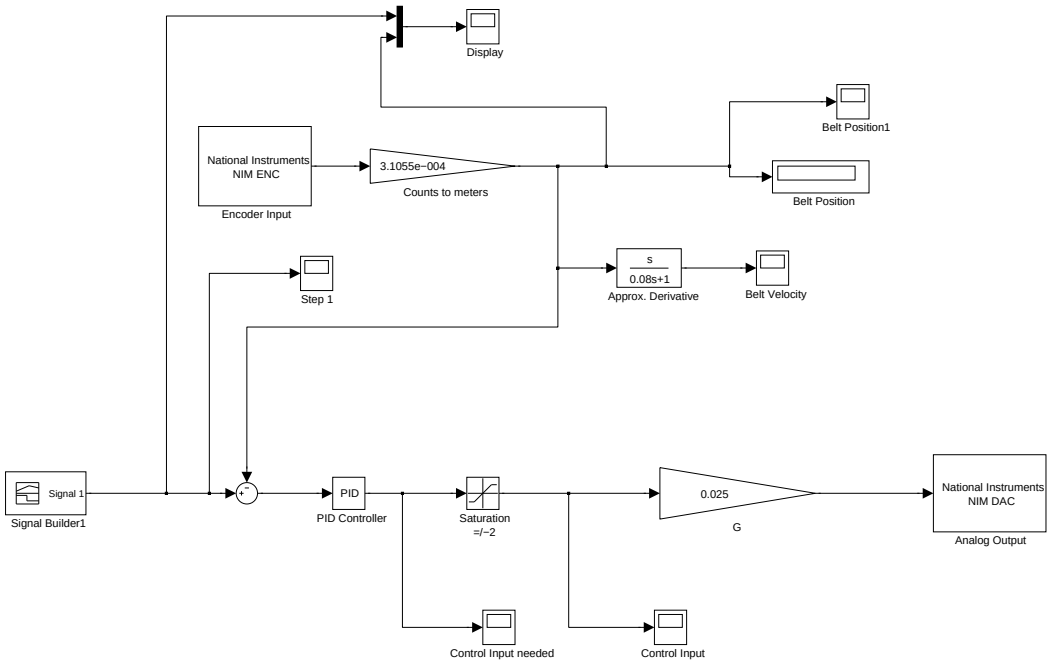

Figure 5.40: Interface of the position control system

Results

A square wave was fed into system in order to simulate movement of an obstacle backward and forward between desired points. The steady state error was always 5 mm or less. Figures 5.41, 5.42, 5.43, 5.44, 5.45 show the test results with displacements of 0.4 m, 0.5 m, 0.6 m, 0.7 m, and 0.8 m respectively.

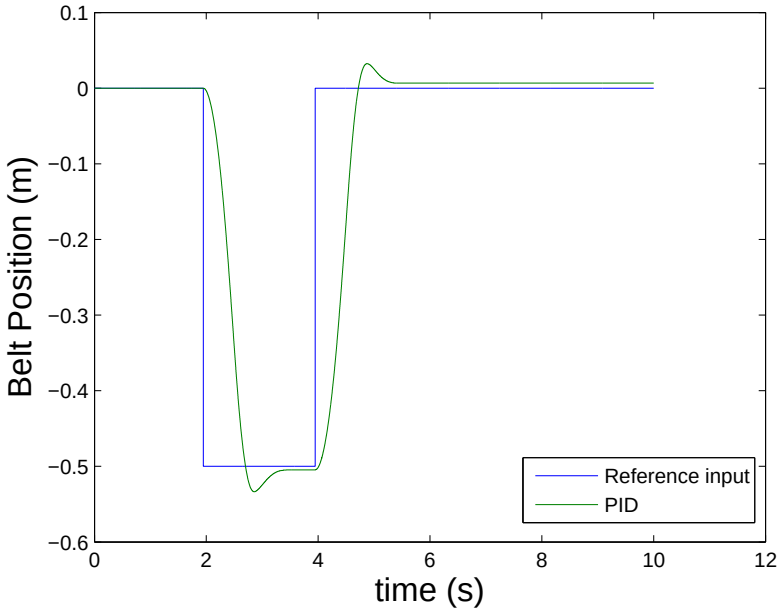

Figure 5.41: Position control test: 0.4m displacement

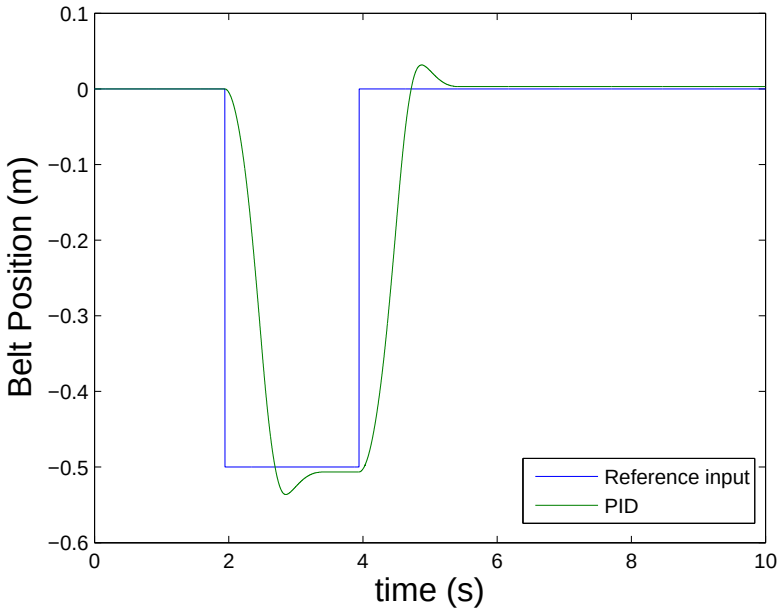

Figure 5.42: Position control test: 0.5m displacement

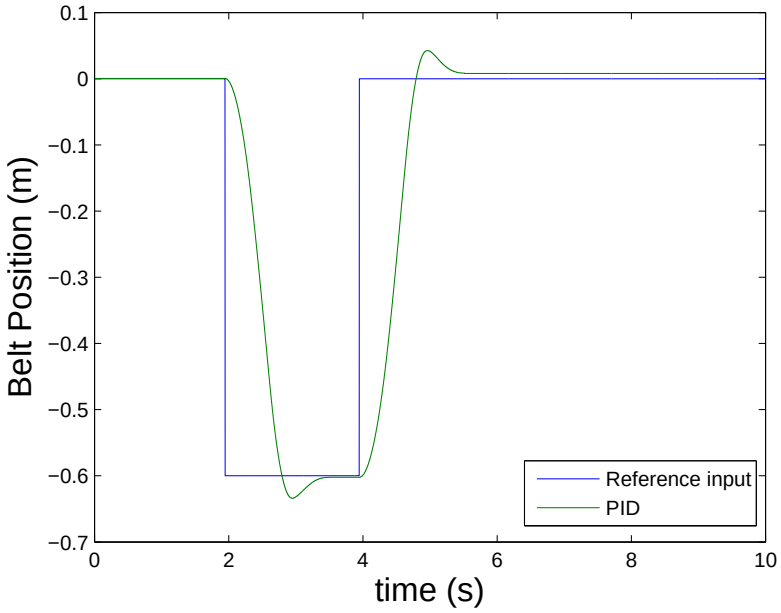

Figure 5.43: Position control test: 0.6m displacement

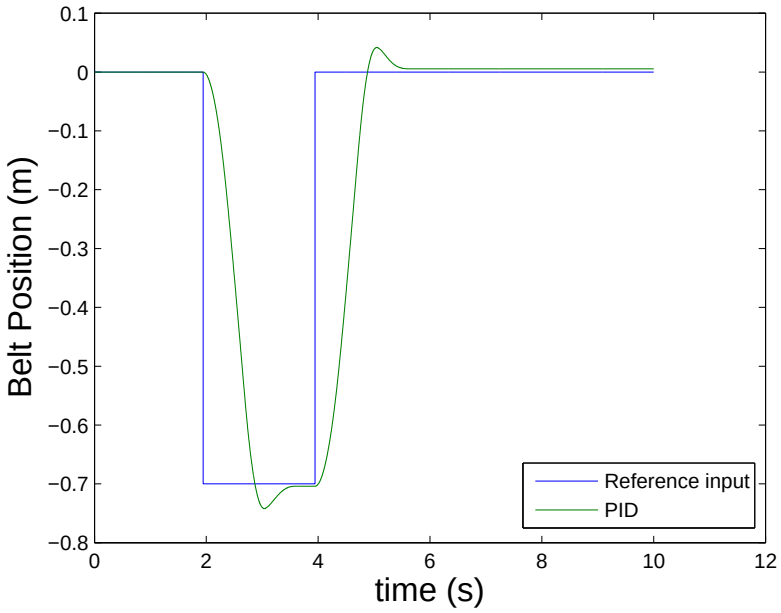

Figure 5.44: Position control test: 0.7m displacement

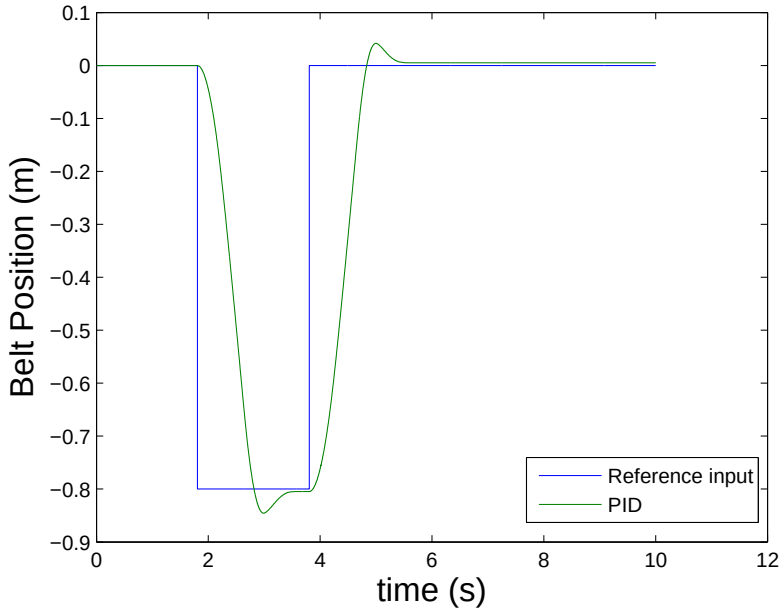

Figure 5.45: Position control test: 0.8m displacement

5.4 Tests with Prosthetic Leg and Robotic Hip Simulator

One of the main objectives of this thesis was to control treadmill speed during tests involving a prosthetic leg and a robotic hip simulator. First of all, step input is fed into system and the treadmill started running, then the hip simulator started running and the prosthetic leg stepped up treadmill. For original controller, the same speed chosen from its own interface. Performances of the controllers is tested while the leg walks on the treadmill.

5.4.1 Results

All tree controllers (PID, SMC, and original conroller) were tested at a speed of 0.84 m/s (1.9 miles/h). The PID gains were tuned as 300, 950, and 0 respectively. The

SMC gains were chosen as: $\lambda = 90$, $\eta = 160$, and $\phi = 0.8$. Figures 5.46, 5.47, and 5.48 show the test results with the PID, SMC, and original controllers respectively. Both PID and SMC had better performance than the original. Figures 5.49, 5.50, and 5.51 show the errors with the PID, SMC, and original controllers respectively. The maximum error was 21×10^{-3} m/s or less for PID controller when the leg applied force on treadmill. It was 16×10^{-3} m/s or less with the SMC controller. And it was 13×10^{-2} m/s for original controller which including 4×10^{-2} m/s offset error. Also, Figures 5.52, 5.53, and 5.54 show thigh angle during tests with prosthethic leg with the PID, SMC, and original controllers respectively. Figures 5.55, 5.56, and 5.57 show knee angle during tests with prosthetic leg with the PID, SMC, and original controllers respectively.

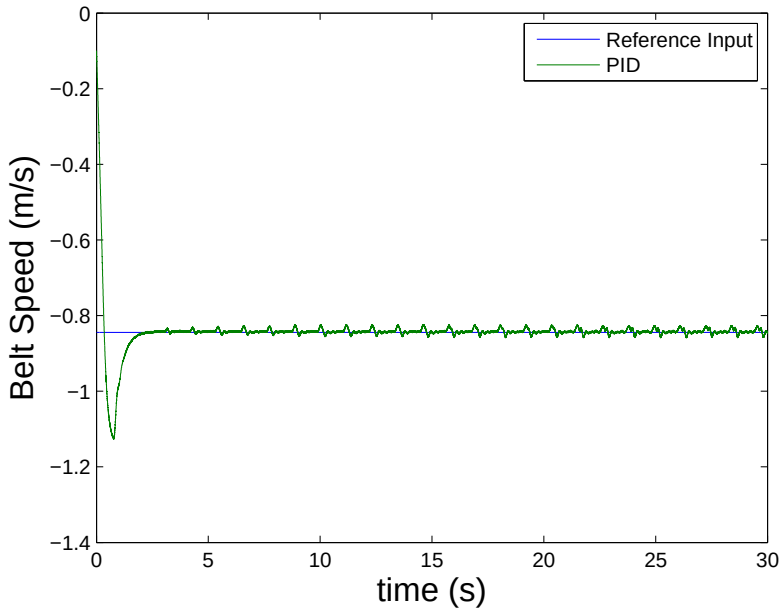

Figure 5.46: PID controller test with prosthetic leg and robot at speed of 0.84 m/s

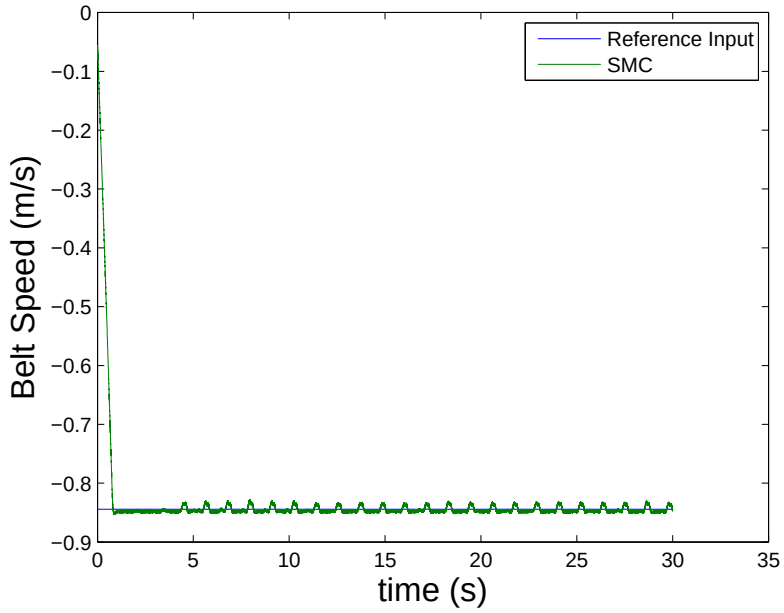

Figure 5.47: SMC controller test with prosthetic leg and robot at speed of 0.84 m/s

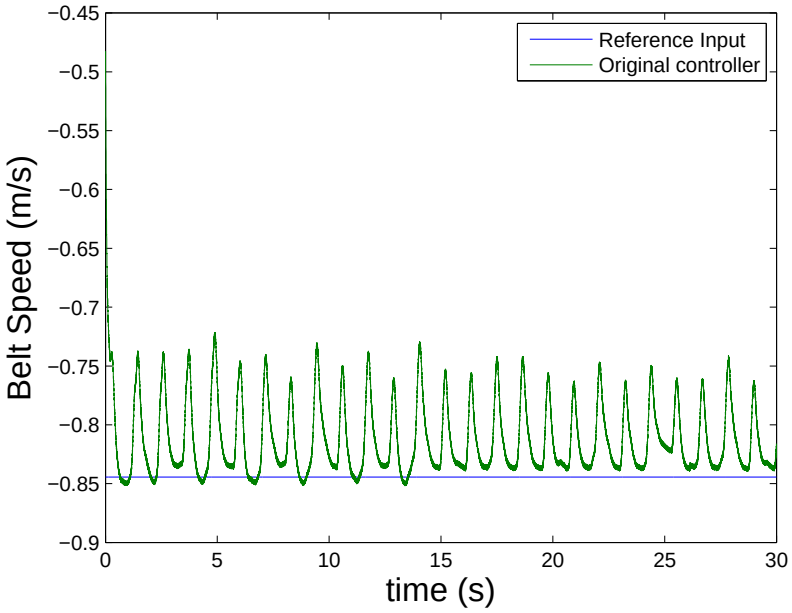

Figure 5.48: Original controller test with prosthetic leg and robot at speed of 0.84 m/s

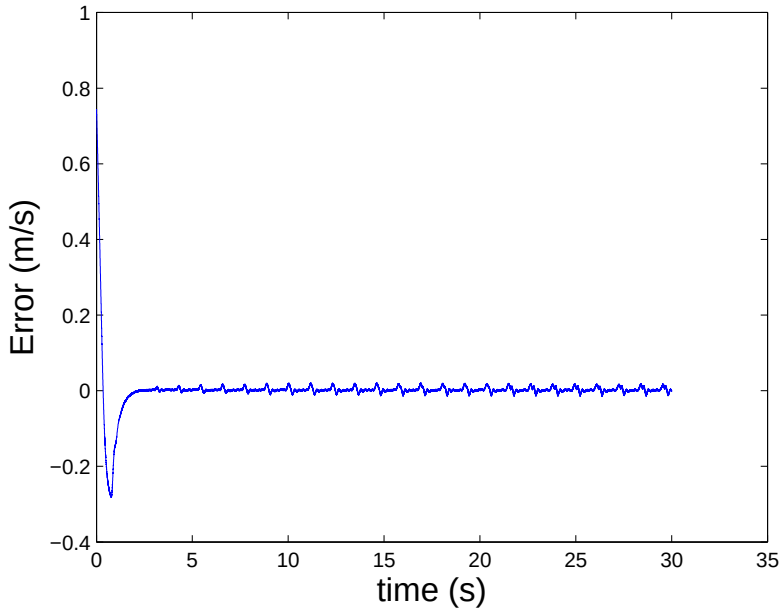

Figure 5.49: Error of PID controller

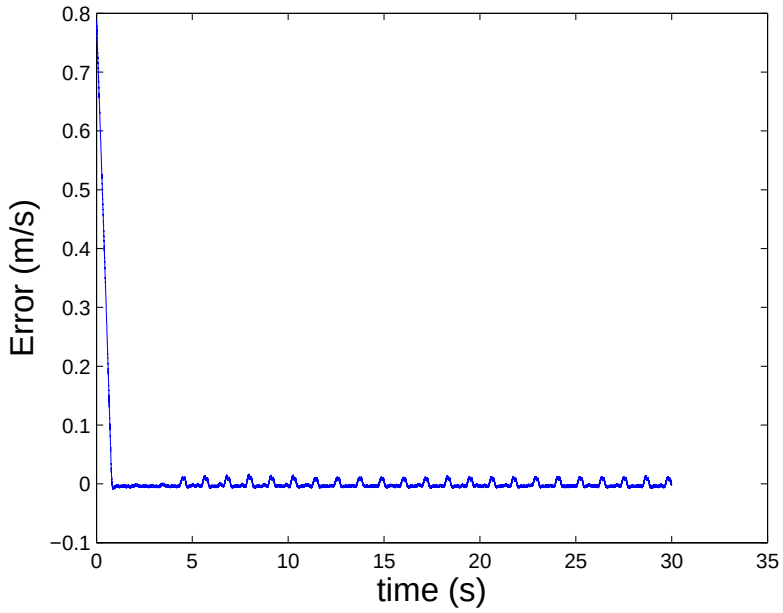

Figure 5.50: Error of SMC controller

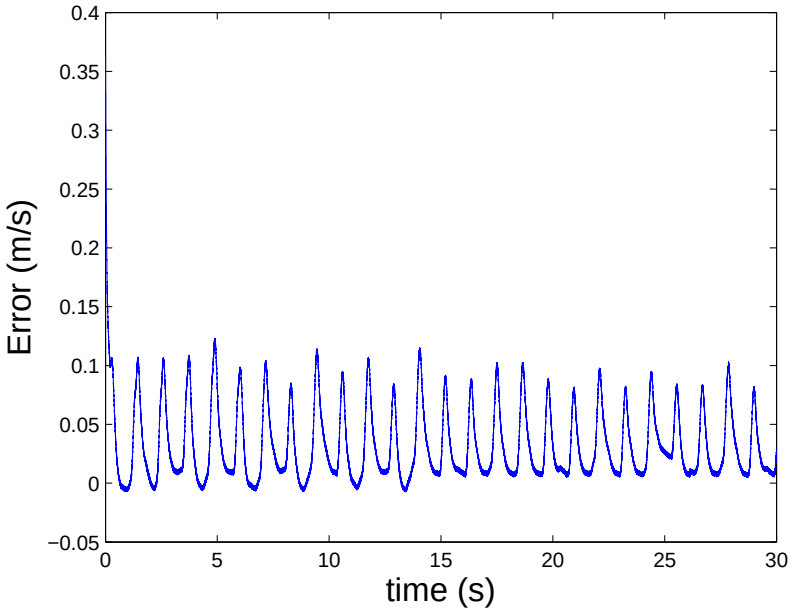

Figure 5.51: Error of original controller

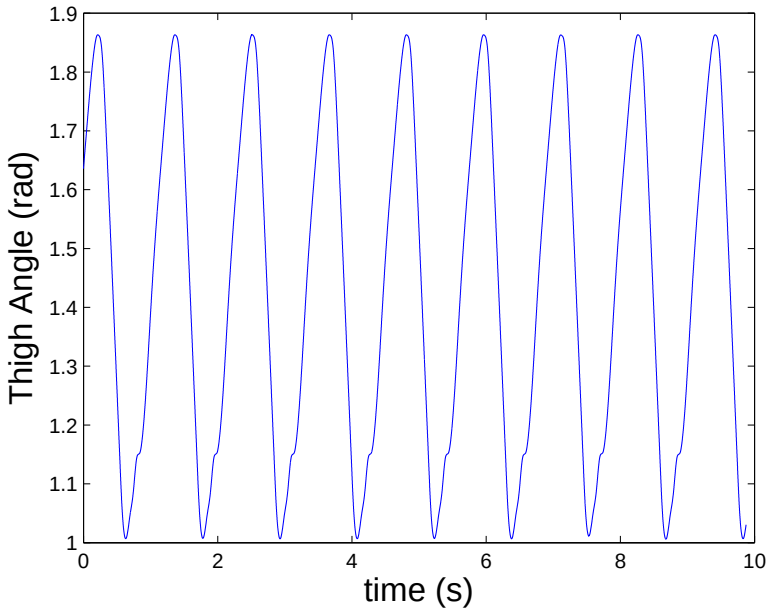

Figure 5.52: Thigh angle during test with prosthethic leg with PID

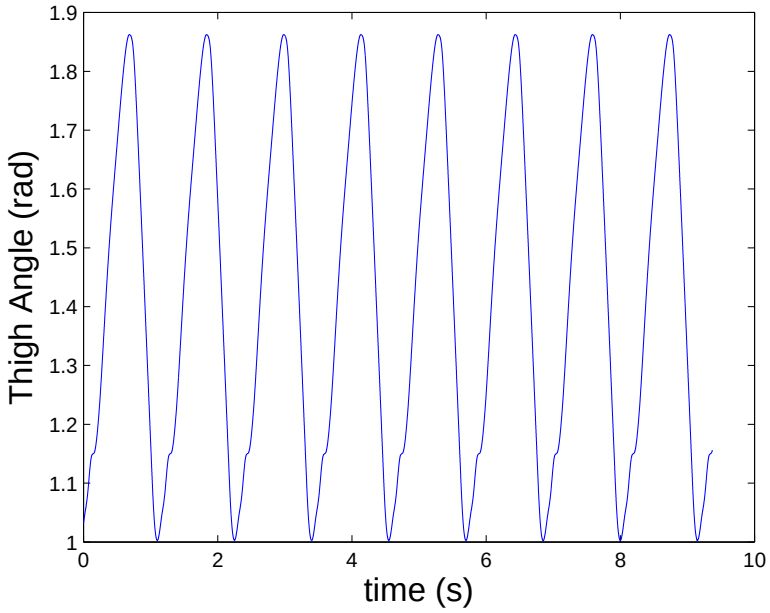

Figure 5.53: Thigh angle during test with prosthethic leg with SMC

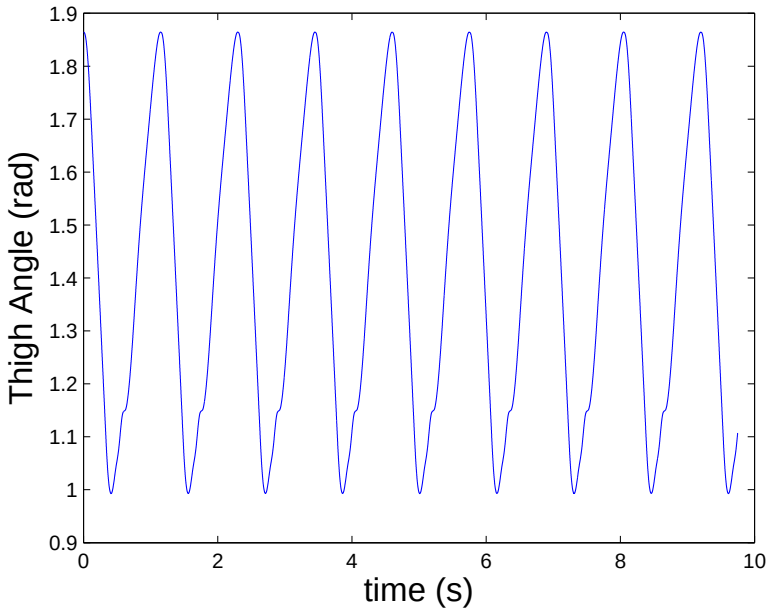

Figure 5.54: Thigh angle during test with prosthethic leg with original controller

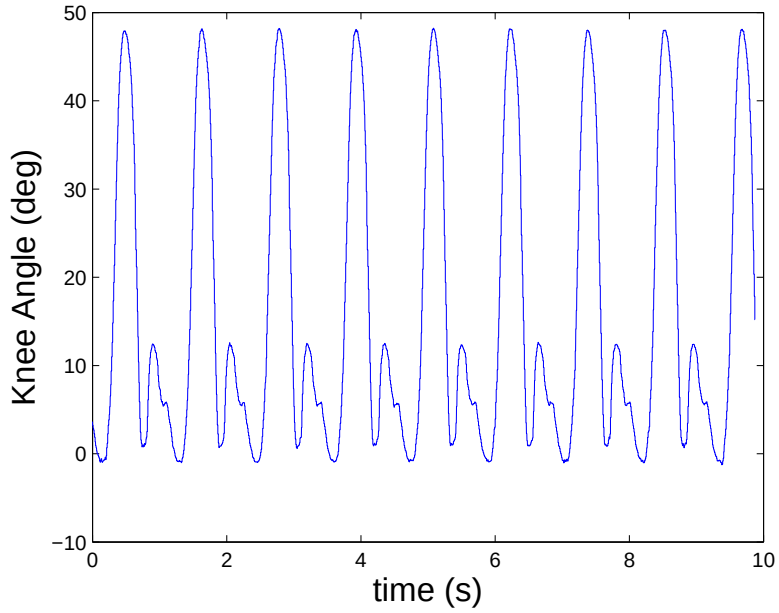

Figure 5.55: Knee angle during test with prosthethic leg with PID

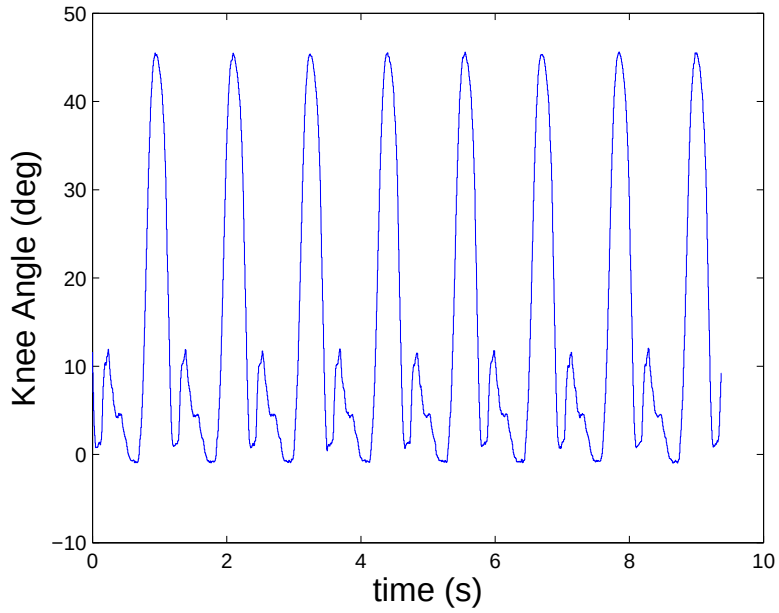

Figure 5.56: Knee angle during test with prosthethic leg with SMC

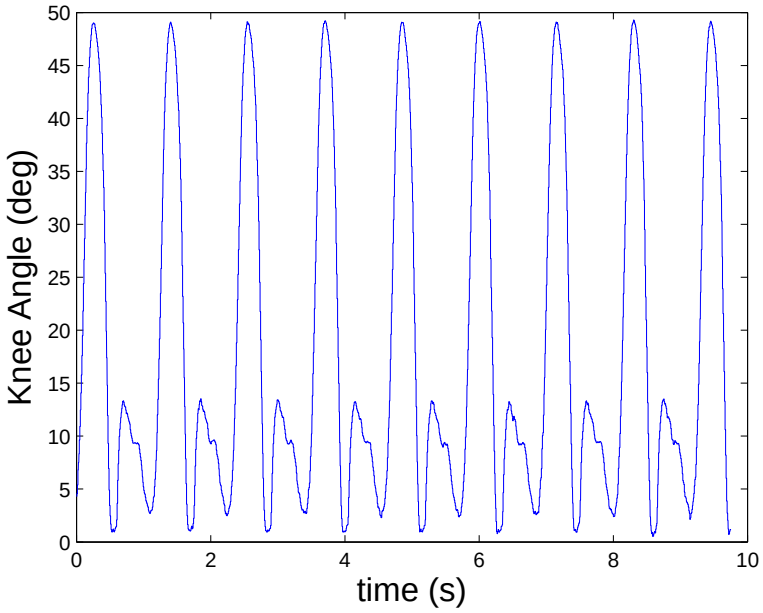

Figure 5.57: Knee angle during test with prosthethic leg with original controller

5.4.2 Root Mean Square of the Error

Root mean square (rms) of the error is calculated by using Eq (5.1) for constant speed, acceleration and deceleration tests in both direction. Table 5.1 shows the rms results for the PID and the SMC.

$$e_{rms} = \sqrt{\frac{\sum e^2(t)}{T}} \tag{5.1}$$

Test	PID	SMC
Constant speed test with a speed of 1.5 mile/h with the subject moving forward	0.0291	0.0626
Constant speed test with a speed of 1.5 mile/h with the subject moving backwards	0.0477	0.0532
Acceleration and deceleration test results with slope of 0.45 m/s^2, with the subject moving forward	0.0091	0.0098
Acceleration and deceleration test results with slope of 0.45 m/s^2, with the subject moving backwards	0.0163	0.0109

Table 5.1: RMS of the error with PID and SMC for constant speed, acceleration and deceleration tests

CHAPTER VI

CONCLUSION AND RECOMMENDATIONS

The main objective of this thesis was to extend the capabilities of a conventional exercise treadmill by providing an external controller. A bond graph-based symbolic model and system identification were combined to estimate relevant transfer functions. Two different control algorithms, namely proportional-integral-derivative and sliding mode, were implemented in the system. Real-time experiments for different conditions such as constant speed, accelerations and decelerations, walking with disturbance like wind, lower speeds for rehabilitation purposes, position control, and test with a prosthethic leg were conducted. Based on simulations and test results, both controllers were adequate for low-power conditions. However, when power requirements were higher due to higher speeds or loads, performance was reduced. Both PID and SMC were better than the original controller in all cases, not only with the prosthesis. There was a slight difference between PID and SMC. The results were more chattering with the PID. For example, in constant speed tests, belt speed oscillated above and below the reference with each step with the the PID controller. However, belt speed was slightly lower than the reference during foot contact, but no overshoot was observed after each step with the SMC. The system with SMC showed better

tracking in some cases such as acceleration and deceleration test. Implementing PID was easier than SMC because of the fact that more calculations were involved with SMC.

6.1 Recommendations

This thesis provides a good viewpoint about controlling a treadmill and it can be implemented on other treadmills. The only restriction was insufficient power for this project. A better power supply can be used for future tests. Also, the controllers can be included in prosthetic leg and robotic hip simulator to provide synchronized movement of treadmill with the leg. An obstacle can also be mounted on the belt, and it can be synchronized with the hip simulator to examine its performance. Also, a sensor may be implemented to estimate the force applied by the leg on the treadmill and the disturbance can be avoided to reduce the error during foot contact.

BIBLIOGRAPHY

[1] 20-sim program. `http://www.20sim.com`.

[2] R.H. Bishop. *The Mechatronics Handbook*. Prentice Hall, 2002.

[3] J.F. Broenink. Introduction to physical systems modelling with bond graphs. http://masters.donntu.edu.ua/2011/fknt/molodih/library/notmy3.pdf, 1999.

[4] R.R. Christensen, J.M Hollerbach, Y. Xu, and S.G Meek. Inertial-force feedback for the treadport locomotion interface. *Presence*, 9(1):1–14, 2000.

[5] V. Dietz, M. Trippel, I.K. Ibrahim, and W. Berger. Human stance on a sinusoidally translating platform: balance control by feedforward and feedback mechanisms. *Experimental Brain Research*, 93:352–362, 1992.

[6] R.C. Dorf and R.H. Bishop. *Modern Control Systems*. Prentice Hall, 2010.

[7] A. Duschau-Wicke, von Zitzewitz, A. J. Caprez, L. Lünenburger, and R. Rinener. Path control: A method for patient-cooperative robot-aided gait rehabilitation. *IEEE Transaction on neural systems and rehabilitation engineering*, 18(1):38–48, 2010.

[8] C. Edwards and S.K. Spurgeon. *Sliding Mode Control: Theory and Applications*. Taylor Francis Ltd, 1998.

[9] J Fung, C.L. Richards, F. Malouin, B.J. Mcfadyen, and A. Lamontagne. A treadmill and motion coupled virtual reality system for gait training post-stroke. *Cyber Physchology Behavior*, 9(2):157–162, 2006.

[10] L. Lichtenstein, J. Barabas, R.L. Woods, and E. Peli. A feedback-controlled interface for treadmill locomotion in virtual environments. *ACM Transactions on Applied Perception*, 4(1):1–17, 2007.

[11] L. Ljung. *System Identification Theory for the User*. Prentice Hall, 1987.

[12] A.E. Minetti, L. Boldrini, L. Brusamolin, P. Zamparo, and T. McKee. A feedback-controlled treadmill (treadmill-on-demand)and the spontaneous speed of walking and running in humans. *Journal of Applied Physiology*, 95:838843, 2003.

[13] E.J Protas, K. Mitchell, A. Williams, H Qureshy, K Caroline, and E.C Lai. Gait and step training to reduce falls in Parkinson's disease. *NeuroRehabilitation*, 20:183–190, 2005.

[14] K.J. Åström and Hägglund. *PID Controllers: Theory, Design, and Tuning*. Research Triangle Park, NC, 1995.

[15] H. Richter, D. Simon, W. Smith, and S. Samorezov. Dynamic modeling and parameter estimation of a leg prosthesis test robot. *in review, Applied Mathematical Modelling*, 2013.

[16] J.L. Souman, P.R. Giordano, I. Frissen, A. De Luca, and M.O. Ernst. Making virtual walking real: perceptual evaluation of a new treadmill control algorithm. *ACM Transactions on Applied Perception*, 7(2):11:1–14, 10.

[17] M.W. Spong, S. Hutchinson, and M. Vidyasagar. *Robot Modeling and Control*. John Wiley Sons, 2006.

[18] A. Stavar, L.M. Dascalu, and D. Talaba. A control system approach for a treadmill walking compensation design. *Bulletin of the Transilvania University of Braşov*, 3(52):129–136, 2010.

[19] V.I. Utkin, J. Guldner, and J. Shi. *Sliding Mode Control in Electromechanical Systems*. Taylor Francis, 1999.

[20] J. von Zitzewitz, M. Bernhardt, and R. Riener. A novel method for automatic treadmill speed adaptation. *IEEE Transactions on Neural Systems and Rehabilitation Engineering*, 15(3):401–409, 2007.